Arnob Kundu

REALISTIC VEHICLE MOVEMENT MODELS AND CORRESPONDING RADIO CHANNEL PARAMETRIZATION FOR THE USE OF POSITIONING AND COMMUNICATIONS STUDIES

Information Technology and
Communication Sciences
Master's Thesis
January 2020

ABSTRACT

ARNOB KUNDU: REALISTIC VEHICLE MOVEMENT MODEL AND CORRESPONDING RADIO CHANNEL PARAMETERIZATION FOR THE USE OF POSITIONING AND COMMUNICATIONS STUDIES
Master of Science Thesis
Tampere University
Master's Degree Program in Wireless Communication
January 2020

Mobility of user equipment introduces significant effects on wireless channel parameters in the context of vehicle movement scenario. In recent years, mobility models being a way of redefining channel parameters in the field of vehicular communication channel has gained noticeable research focus. Furthermore, different performance aspects like throughput, reliability, availability as well as latency require analysis from both real life and simulation point of view. In the thesis scope, vehicle specific mobility models are selected based on algorithm simplicity, reliability and efficiency over other mobility models. In addition, the channel parameters are described and simulated taking user equipment mobility as well as different carrier frequency usage into account. Besides, in the context of vehicular communication regarding different vehicle types it is important to converge mobility models in positioning studies. Moreover, tracking the user position with velocity estimates is simulated and analysed by using Kalman filter methodology to illustrate the effect of user equipment velocity on the filtering scenario. Furthermore, effect of base station geometry on channel performance with reference to the mobility path of user equipment in the context of different carrier frequency usage is simulated and discussed to portray variation in the channel throughput. Finally, different channel modelling parameters are considered maintaining contextual resemblance with the mobility models to analyse as well as simulate different scenarios related to vehicle mobility effect on channel parameters.

Keywords: Mobility models, Channel model, Fast fading, Doppler spread, Delay spread, Kalman filter methodology

PREFACE

This thesis was conducted as a requirement for the Degree Program Master of Science in Wireless Communication at Tampere University. The writing and simulation procedures were conducted under the supervision of University lecturer Jukka Talvitie and examined together with Professor Mikko Valkama. I would like to thank both of them cordially for their constant support and guidance. Finally, I would love to thank my parents for their guidance, patience and support throughout my whole life.

Tampere, 29 January 2020

Arnob Kundu

CONTENTS

LIST OF FIGURES

LIST OF SYMBOLS AND ABBREVIATIONS

UAV	Unmanned Aerial Vehicle
UMa	Urban Macro
LOS	Line of Sight
NLOS	Non Line of Sight
RMS	Root Mean Square
MIMO	Multiple Input Multiple Output
cmWave	centimetre wave
mmWave	millimetre wave
TTI	Transmit Time Interval
EIM	Element Increment Method
RW	Random Walk
RWP	Random Waypoint
RD	Random Direction
EFK	Extended Kalman Filter
5G NR	5G New Radio
MANET	Mobile Ad-hoc Networks
dB	decibels
P_{loss}	path loss
$f_{carrier}$	carrier frequency
h_{mobile}	mobile antenna height
h_{base}	base station antenna height
PL_{LOS}	path loss for line of sight
PL'_{NLOS}	path loss for non-line of sight
f_{RX}	received frequency
f_{TX}	transmitted frequency
f_D	Doppler shift
f_d	Doppler frequency shift
V_{mobile}	velocity of moving object
$\lambda_{carrier}$	corresponding wavelength of carrier frequency
f_{max}	maximum Doppler frequency shift
S_e	Doppler spectrum
V_i	initial speed
V_f	final speed
t_a	acceleration time
X_a	acceleration distance
t_d	deceleration time
X_d	deceleration distance
C	net force of a train
F_y	force of traction
W	force of resistance
B	braking force
M	total mass of train
σ	Gaussian noise variance
A	correlation parameter
$N(.)$	multivariate normal distribution
σ_{pos}	standard deviation of position measurement error
σ_{acc}	rate of change parameter
X_{bs}	base station position in x-axis with reference to the movement path
Y_{bs}	base station position in y-axis with reference to the movement path

1. INTRODUCTION

Mobility models refer to the characterization of vehicle or user movement in the context of location, velocity and heading direction with a course of time. Besides, designing of mobility models depends on the vehicle classification as well as vehicle movement environment. Mobility models are considered as the foundation of analysing the effect of varying radio channel parameters concerning positioning and communication studies in the context of user mobility. Communication channel models and their properties vary with the mobility of user equipment as a resultant of change in different performance aspect, throughput, latency, reliability and availability. Moreover, mobility models play significant role in trace-based positioning like Kalman filtering methodology [1].

User mobility effect on wireless channel parametrization has gained interest in the recent times, as need for vehicular communication is on the rise. Besides, autonomous vehicles have been in the centre of interest in recent years. Hence, redefining channel parameters as well as redesigning of communication links based on different performance aspect analysis is important for future studies in the field of positioning and communication studies. Therefore, in this thesis scope, basic mobility models concerning different vehicles like, cars, high speed trains, unmanned aerial vehicles or drones as well as pedestrian mobility models are described and analysed through simulation scenario.

Numerous recent works have been done regarding mobility models in the context of vehicular communication. A recent work [2] has introduced formation control or formation in motion describing control actions to ensure that certain group of vehicles maintains fixed or dynamic pattern during movement. Regarding high speed train communication system, a survey based work [3] on channel measurement for high speed train is conducted to outline channel measurement model as well as other research direction.

In this thesis scope, a feasibility analysis is done for the selected mobility models concerning different vehicle types. Besides, different channel parameters are described in the context of mobility of user equipment. Mobility of user equipment is considered in the context of acceleration, deceleration as well as constant speed scenario of the specific vehicle. Moreover, analysing different channel parameters is performed regarding different frequency bands. On the other hand, in the context of tracking user position through

mobility model analysis, Kalman filtering methodology is adopted to illustrate the tracked velocity and positioning accuracy.

Contribution of author to the thesis are listed as follows,

- Literature review on channel models and parameters in the context of mobility
- Literature review on vehicle mobility models in a comparative overview as well as performing simulation of the mobility models under different scenarios
- Simulations of communications channel with studied mobility models
- Simulations of using the mobility models for tracking with Kalman filter
- Analysis and discussion considering the effects of mobility on the communication channel properties

Remaining part of this thesis is structured as follows,

In chapter two, basic communication channel models and parameters are described, simulated and evaluated from mobility point of view. Then, chapter three includes the selected mobility model algorithm representation for different vehicle types as well as simulation regarding different scenarios. After this, chapter four describes the positioning and tracking aspects concerning mobility models through tracking algorithm like Kalman filter methodology. Moreover, in chapter five effect of mobility on channel parameters is simulated and illustrated through figures. Finally, conclusion and discussion regarding future aspects of mobility modelling in the context of radio channel parametrization as well as vehicular communication are provided in chapter six.

2. BASICS OF COMMUNICATION CHANNEL MODELS AND PARAMETERS

2.1 Channel Modelling Principles

In time domain representation a channel model is defined as the impulse response regarding channel medium through which signals are being propagated, whereas in the frequency domain it is defined as the Fourier transformation of the impulse response. In other words, channel model is a mathematical representation of the channel medium [4]. Choosing the correct channel model is essential for link performance optimization, analysing trade-offs regarding system architecture and providing a practical overview of system performance.

Regarding these applications, A. Molisch [5] suggests three channel modelling methods, namely, stored impulse response dependent, deterministic and stochastic channel model. Main advantage of stored impulse response based approach is reusable real life data where the disadvantage lies in the complex procedure for acquiring and storing data characterizing a certain area rather than the whole propagation environment. Besides, stochastic models are preferred for system design and comparison whereas the deterministic or site-specific models are focused on planning and system deployment. Finally, in this section, among different channel models, path loss models, slow fading and fast fading models are discussed. The fast fading is closely related to the thesis scope as this is in close vicinity in the context of mobility modelling. Besides, the fading model discussed in the thesis scope is stochastic in nature as the data generation is random whereas in context of vehicle movement the path loss model is deterministic in nature.

2.1.1 Path loss models

Path loss is the difference between transmitted and received power, typically given in dB (decibels), representing attenuation of signal level caused by free space propagation, diffraction, reflection and scattering [6]. Path loss models are designed for determining strength of received signal and consider the average of both small and large scale fading scenarios. Three kinds of path loss models, namely; Empirical, Semi-deterministic and deterministic model [5]:

- Empirical models- more simplistic in nature, these models provide poor accuracy based on measurement data and statistical properties only.
- Semi-deterministic models- more deterministic aspects than empirical models.

- Deterministic models- great accuracy, require enormous site specific geometry data, large computational load and complex in nature.

One of the most popular empirical models is Okumura-Hata model. Path loss according to Okumura-Hata [5] is as follows,

$$P_{loss} = \alpha + \beta \log(D) + \gamma \tag{2.1}$$

where, *α, β, γ* are three factors dependent on carrier frequency as well as base station and mobile antenna heights, *D* is the distance between two antennas and Ploss is scaled in dB.

$$\alpha = 69.55 + 26.16 \log(f_{carrier}) - 13.82 \log(h_{base}) - a\,(h_{mobile}) \tag{2.2}$$

$$\beta = 44.9 - 6.55 \log(h_{base}) \tag{2.3}$$

Here, the $f_{carrier}$ is in MHz, *D* is in kilometres, h_{mobile} and h_{base} is in meters. The function $a(h_{mobile})$ and factor γ is propagation environment dependent.

For urban areas,

$$a(h_{mobile}) = \left(1.1 \log\left(f_{carrier}\right) - 0.7\right)h_{mobile} - \left(1.56 \log\left(f_{carrier}\right) - 0.8\right) \tag{2.4}$$

$$\gamma = 0 \tag{2.5}$$

For metropolitan areas,

$$\gamma = \begin{cases} 8.29(\log(1.54h_{mobile}))^2 - 1.1 & for\ f_{carrier} \leq 200MHz \\ 3.2(\log(11.75h_{mobile}))^2 - 4.97 & for\ f_{carrier} \geq 400MHz \end{cases} \tag{2.6}$$

$$\gamma = 0 \tag{2.7}$$

For suburban areas,

$$\gamma = -2\left[\log\left(\frac{f_{carrier}}{28}\right)\right]^2 - 5.4 \tag{2.8}$$

For rural areas,

$$\gamma = -4.78\left[\log\left(f_{carrier}\right)\right]^2 + 18.33 \log\left(f_{carrier}\right) - 40.98 \tag{2.9}$$

The function $a(h_{mobile})$ in suburban and rural areas are same as urban areas. Noticeably, the Okumura-Hata model covers the frequency range for microwave frequencies i.e. up to 1500 MHz. A simulation scenario depicting the effect of different distance between base station and mobile station antenna along with different base station antenna height is illustrated in Figure 1 below, where the carrier frequency chosen is 1000 MHz along with three different base station heights, 30 m, 100 m and 200 m in the context of three different propagation environment namely, large urban, suburban and rural area.

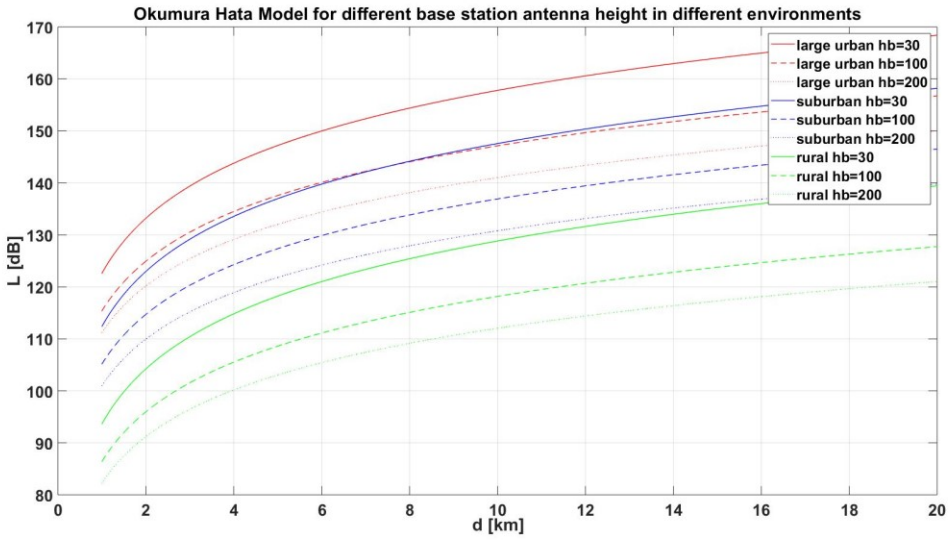

Figure 1. *Effect of distance between base station and mobile station antennas along with different base station antenna heights on path loss (dB) in different propagation environments*

However, with the increasing demand on frequency bandwidth as well as already clattered up existing frequency band new bands are coming into consideration regarding the 5G communication technologies. In the article, '3GPP TR 38.901 version 15.1.0' [7] channel model regarding frequency range from 0.5 to 100 GHz is discussed. The Urban Macro (UMa) scenario is discussed in more detail as it concedes better with the mobility modelling context in urban areas. Regarding LOS (line of sight) scenario where log normal shadow fading, $\sigma_{SF} = 4\ dB$,

$$PL_{LOS} = \begin{cases} PL_a & 10m \le d_1 \le d_{bp}^{'} \\ PL_b & d_{bp}^{'} \le d_1 \le 5km \end{cases} \tag{2.10}$$

Here,

$$PL_a = 28.0 + 22\log_{10}(d_2) + 20\log_{10}(f_{carrier}) \tag{2.11}$$

$$PL_b = 28.0 + 40\log_{10}(d_2) + 20\log_{10}(f_{carrier}) - 9\log_{10}\left(\left(d_{bp}'\right)^2 - (h_{base} - h_{mobile})^2\right) \tag{1.12}$$

Regarding, NLOS scenario, where log normal shadow fading, $\sigma_{SF} = 6\ dB$,

$$PL_{NLOS} = \max(PL_{LOS}, PL'_{NLOS}) \qquad 10\ m \le d_1 \le 5\ km \tag{2.13}$$

where,

$$PL'_{NLOS} = 13.54 + 39.08\log_{10}(d_2) + 10\log_{10}(f_{carrier}) - 0.6(h_{mobile} - 1.5) \tag{2.14}$$

Additionally, an optional path loss model considering $\sigma_{SF} = 7.8\ dB$, in this context,

$$PL = 32.4 + 20\log_{10}(f_{carrier}) + 30\log_{10}(d_2) \tag{2.15}$$

In both LOS and NLOS scenarios, height of mobile or user terminal and base-station is, $1.5m \leq h_{mobile} \leq 22.5m$ and $h_{base} = 25m$. The distance $\boldsymbol{d_1}$ $\boldsymbol{and}$ $\boldsymbol{d_2}$ mentioned in equation 2.10-2.15 can be illustrated as follows in Figure 2 below,

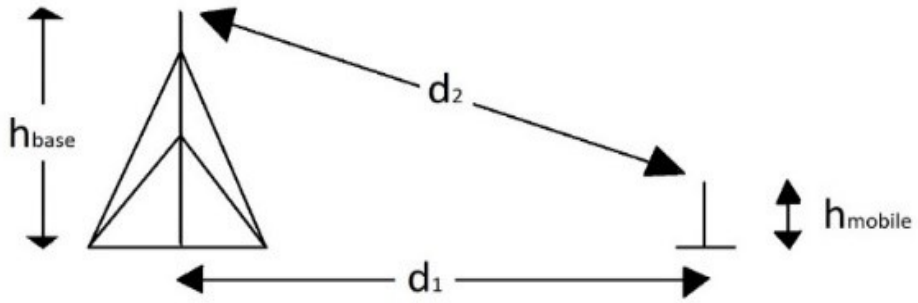

Figure 2. *Diagram for illustrating distances* $\boldsymbol{d_1}$ *and* $\boldsymbol{d_2}$

Another parameter, distance for breakpoint, $d'_{bp} = 4h'_{base}h'_{mobile}f_{carrier}/c$, where, effective antenna heights for base-station and user terminal, $h'_{base} = h_{base} - h_{environmet}$ and $h'_{mobile} = h_{mobile} - h_{environmet}$. Parameter $h_{environment}$ stands for the effective environment height and is 1m in UMa scenario [7] .

2.1.2 **Shadowing/ slow fading model**

Slow fading model varies very slowly with respect to change in frequency. In slow fading phenomenon, absorption of transmission power by objects located between transmitter and receiver is observed. Besides, the phenomenon takes place when the receiver is located indoor and the transmitted wave has to get past the walls to reach the receiver. Moreover, the phenomenon is referred to as shadow fading, as large objects like big buildings or trees can block the direct propagation path between transmitter and receiver resulting in a fade resembling shadow or obstacle in propagation medium [8]. Noticeably, change in channel impulse response is slower than the transmitted signal [9]. In Figure 3, a general representation on the effect of shadowing is illustrated.

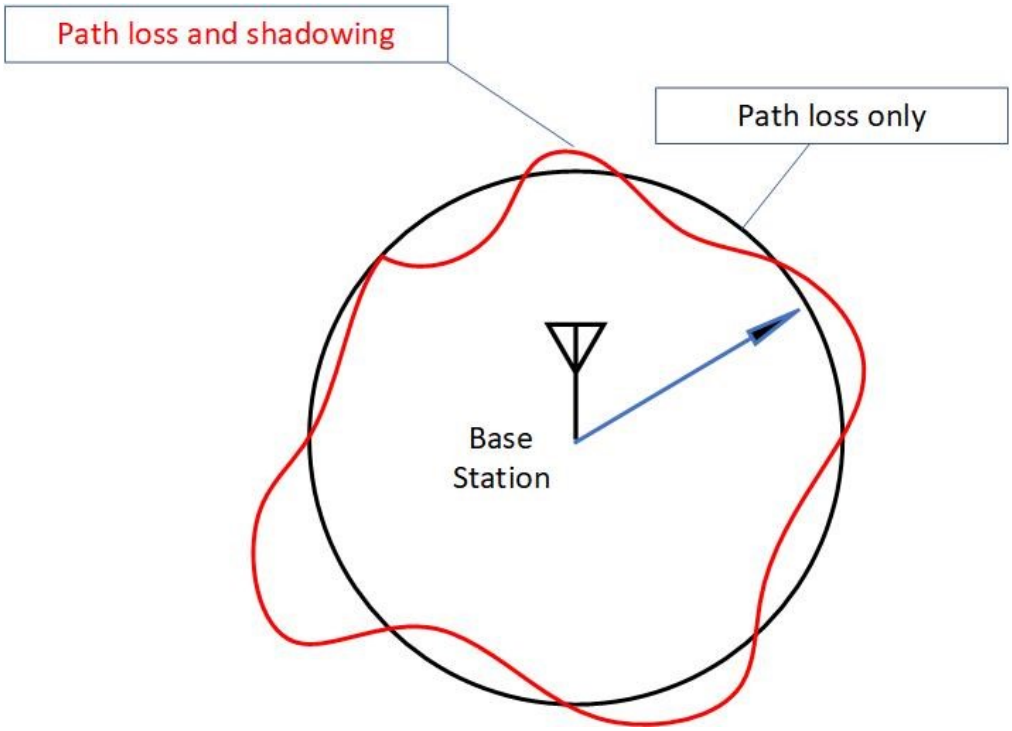

Figure 3. *Effect of shadowing on constant received power contours*

2.1.3 Fast fading model

Fast fading model varies quickly with change in frequency. As a resultant of interference between multiple copies of the original transmitted signal reaching the receiver at different time instants, rapid variation in received signal's amplitude, phase or multipath delays is observed [8]. The phenomenon is resultant of multipath, i.e. effect of constructive and destructive interference patterns originated due to multipath propagation, resulting in power level variation of the received signal. Besides, moving objects in the propagation medium may cause fast fading even if the transmitter and receiver are stationary [10]. Noticeably, in the absence of line of sight path between transmitter and receiver, received signal in a fast fading model follows Rayleigh distribution and in the presence of one line of sight path Rician distribution is followed [8].

2.2 Doppler Effect

This phenomenon is caused by the movement of either transmitter, receiver or both, as well as other objects present in a propagation medium. This relative movement causes the frequency to shift at the receiver than the original signal frequency at the transmitter. This scenario can be furthermore explained by the following simple equation,

$$f_{Rx} = f_{Tx} \pm f_D \tag{2.16}$$

where, f_{Rx} is the frequency at the receiver, f_{Tx} is the frequency at the transmitter and f_D is the Doppler shift. (+) sign is valid if the transmitter and receiver is moving closer to each other while the $(-)$ sign is valid if the transmitter and receiver are moving farther away from each other. The Doppler frequency shift [5] is given as,

$$f_d = \frac{V_{mobile}}{\lambda_{carrier}} cos\theta \tag{2.17}$$

where, V_{mobile} is the velocity of the moving object such as transmitter or receiver, $\lambda_{carrier}$ is the corresponding wavelength of carrier frequency and θ is the angle between incoming wave and receiver. Doppler frequency shift can attain its maximum value when $cos\theta = 1$ and is denoted by,

$$f_{max} = \frac{V_{mobile}}{\lambda_{carrier}} \tag{2.18}$$

Moreover, the effect of Doppler frequency shift can be illustrated through Jakes' [4] spectrum,

$$S_e(f) = \frac{1.5}{\pi f_{max} \sqrt{1 - \left(\frac{f - f_{carrier}}{f_{max}}\right)^2}} \tag{2.19}$$

where, $f - f_{carrier} = -f_{max} \ldots f_{max}$ denotes the frequency range.

Besides, in the context of Jakes' [11] spectrum, a single sine wave transmission is considered and the received signals from various directions in Figure 4 are arriving with equal probability.

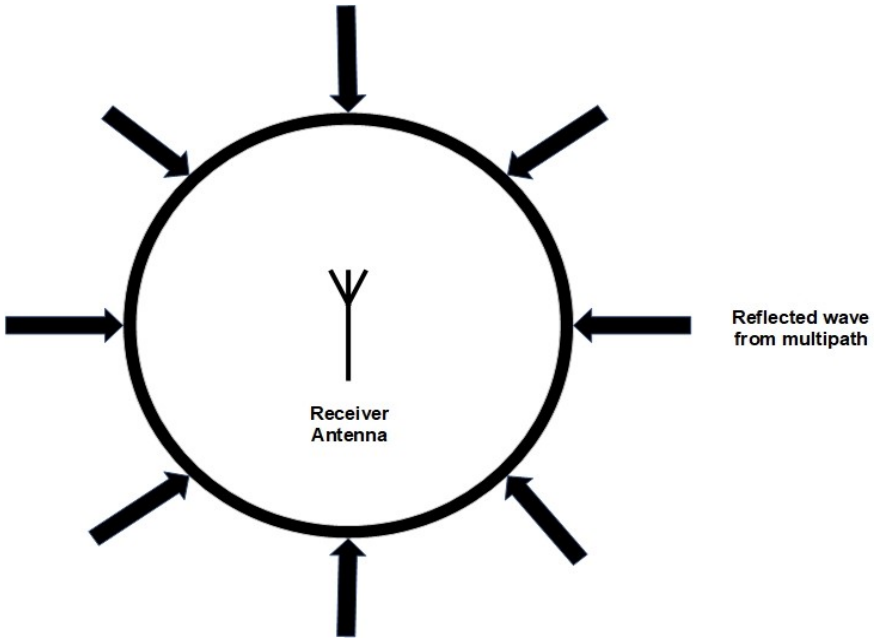

Figure 4. *Reflected wave from multipath arriving with equal probability*

Doppler frequency shift introduces frequency dispersion for received signal as well causes the received signal to have a larger bandwidth than the transmitted signal. In the context of mobility effects on channel models, Doppler phenomenon is dominant in nature. As illustrated in equation 2.18, Doppler frequency shift is directly affected by vehicle speed and carrier frequency. A graphical illustration is shown here for three different carrier frequencies, 800 MHz, 3.5 GHz and 30 GHz while the vehicle speed remains constant at 100 km/h. As illustrated in Figure 5,6 and 7, higher the carrier frequency more spread of Doppler spectrum in frequency domain is observed. The spreading range is between $f_{carrier} - f_{max}$ and $f_{carrier} + f_{max}$ where $f_{carrier}$ lies in the centrum of spread. Moreover, value of f_{max} is dependent on the used carrier frequency. Hence, in the frequency division multiple access technique, with higher carrier frequency larger sub-carrier spacing is required to mitigate the effect of inter sub-carrier interference. Noticeably, considering maximum Doppler frequency shift f_{max}, various angles of incoming waves to the receiver is not considered.

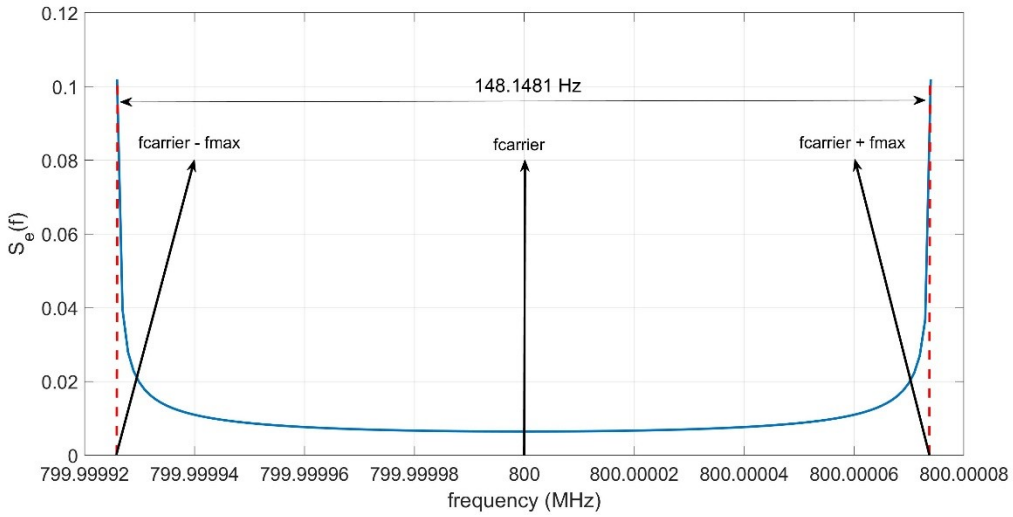

Figure 5. *Doppler spectrum vs frequency (vehicle speed 100 km/h, carrier frequency 800 MHz)*

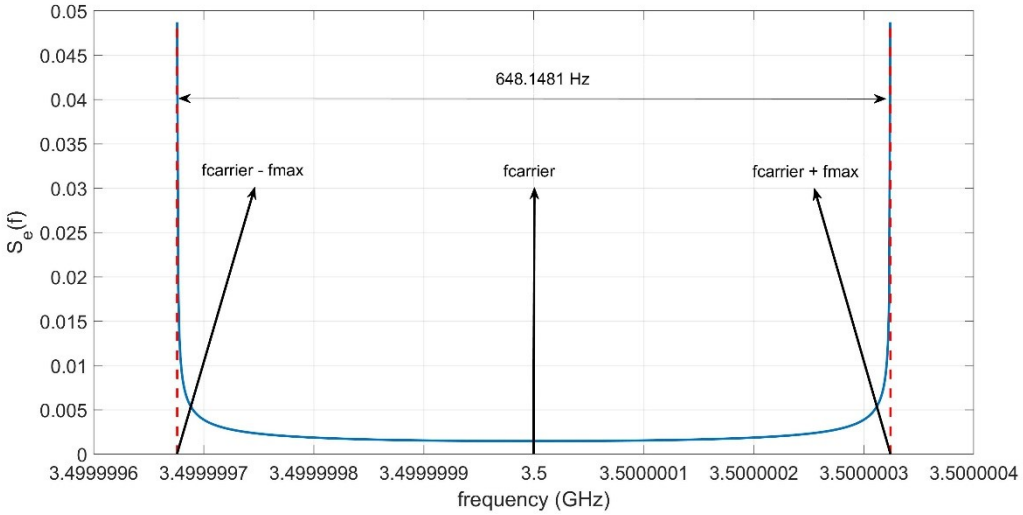

Figure 6. *Doppler spectrum vs frequency (vehicle speed 100 km/h, carrier frequency 3.5 GHz)*

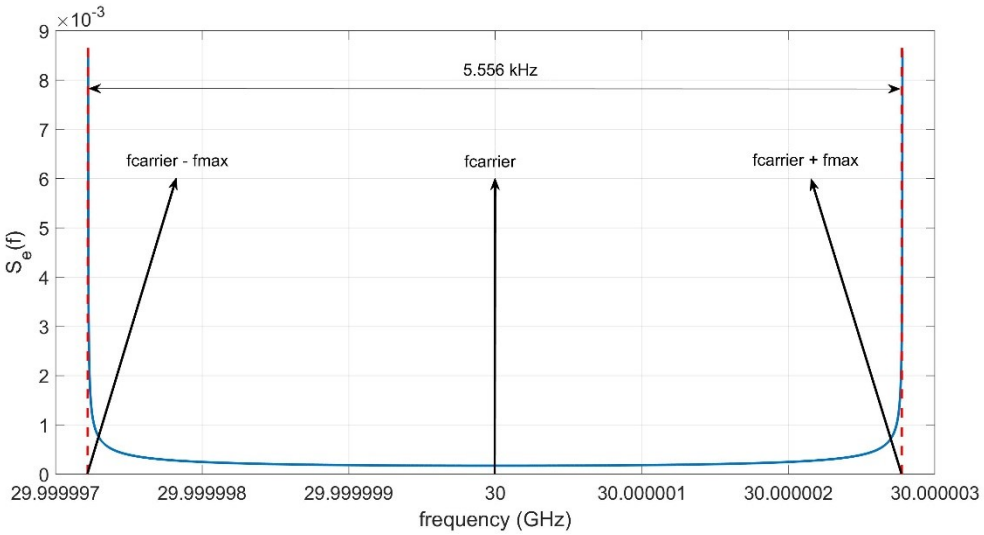

Figure 7. *Doppler spectrum vs frequency (vehicle speed 100 km/h, carrier frequency 30 GHz)*

Finally, from Figure 5, 6 and 7, it can be observed that effect of higher carrier frequency increases the Doppler spread in a drastic manner because of the chosen carrier frequencies, 800 MHz, 3.5 GHz and 30 GHz. Spreading of Doppler spectrum depends on the maximum Doppler frequency shift as well as the vehicular speed from equation 2.18. Hence, keeping the carrier frequency fixed at 3.5 GHz and varying the vehicle speed in

three stages, 60 km/h, 100 km/h and 200 km/h, following results are achieved and therefore illustrated in Figure 8, 9 and 10.

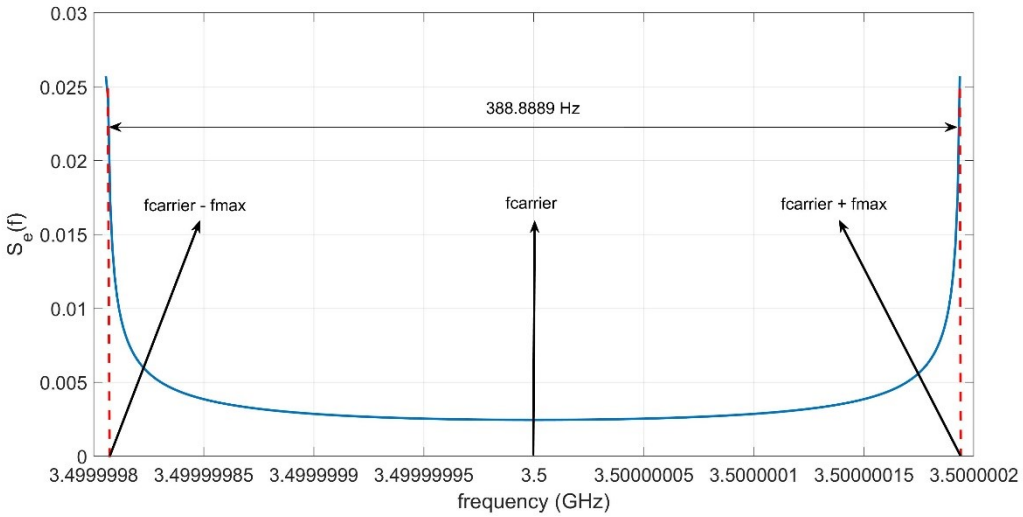

Figure 8. *Doppler spectrum vs vehicle speed (vehicle speed 60 km/h, carrier frequency 3.5 GHz)*

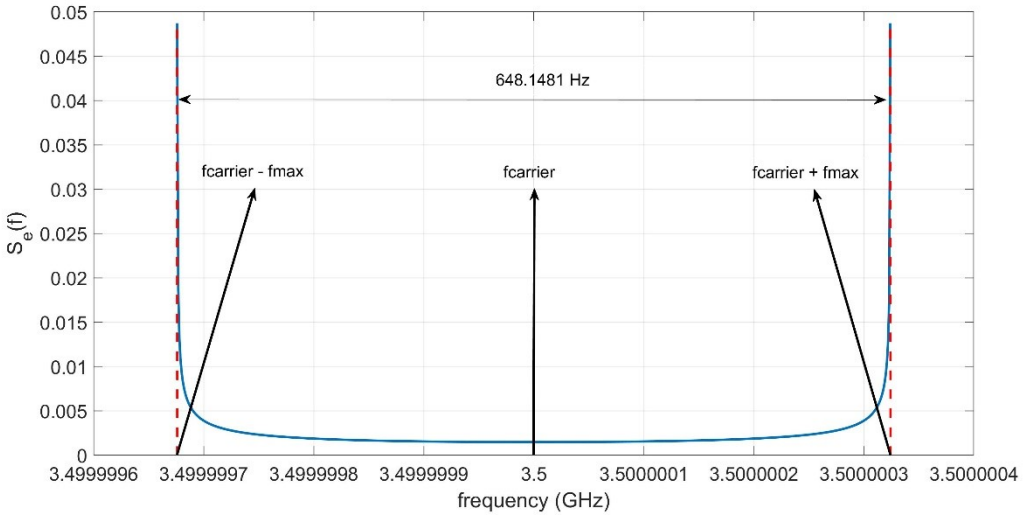

Figure 9. *Doppler spectrum vs vehicle speed (vehicle speed 100 km/h, carrier frequency 3.5 GHz)*

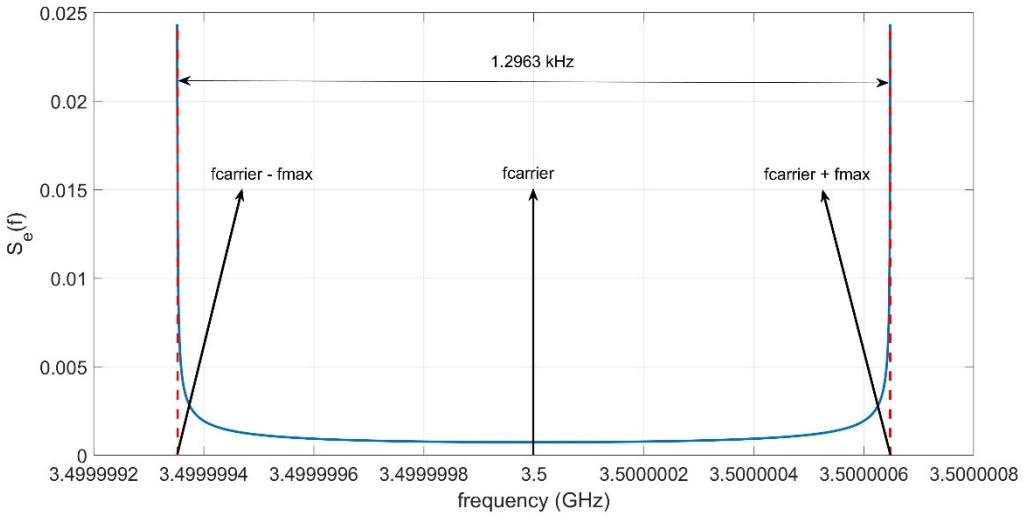

Figure 10. *Doppler spectrum vs vehicle speed (vehicle speed 200 km/h, carrier frequency 3.5 GHz)*

From Figure 8, 9 and 10, it can be seen that spread of Doppler spectrum is increasing with the increase in vehicle speed. The phenomenon explains that with increasing vehicle speed Doppler effect gets dominant. However, the effect of carrier frequency and vehicle speed change on Doppler spread is considered similar. Effect of vehicle speed change is considered linear for a fixed carrier frequency, as example, for 60 km/h, 100 km/h and 200 km/h; f_{max} is consecutively 44 Hz, 74 Hz and 148 Hz; while for a fixed vehicle speed of 100 km/h and carrier frequency of 800 MHz, 3.5 GHz and 30 GHz; f_{max} is consecutively 74 Hz, 324 Hz and 2777.78 Hz. Moreover, taking Rayleigh fading channels into consideration, the effect of f_{max} is dominant on fading scenario as illustrated in Figure 11.

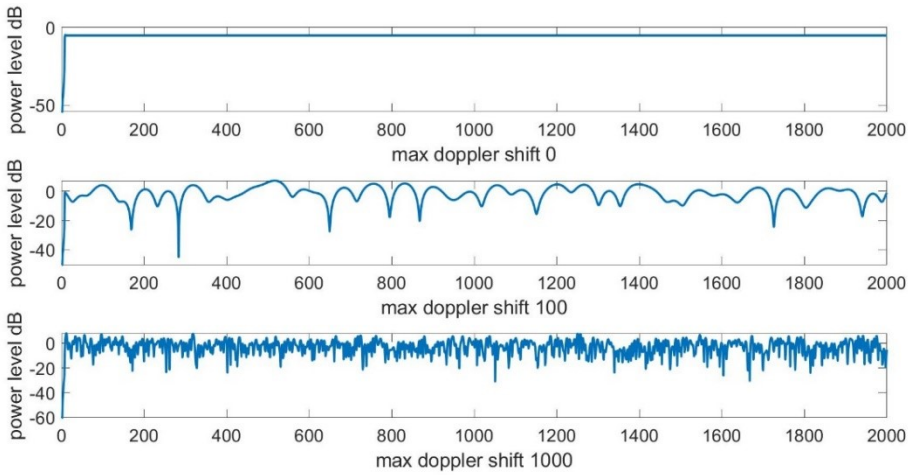

Figure 11. *Example realizations of single-tap Rayleigh channels with different Doppler shifts*

As seen in Figure 11, f_{max} being zero depicts a static channel where fading is almost absent. However, with increasing f_{max}, fading increases.

2.3 Delay Spread

Delay spread can be described as a direct resultant from multipath phenomenon. Different signal paths between transmitter and receiver corresponds to different transmissions delays. Due to multipath an identical signal from transmitter can be received as multiple copies of the transmitted signals at the receiver end. Signal conveyed on the shortest path (typically LOS) reaches the receiver faster than those conveyed on the longer reflected paths due to multipath, which causes signal spreading in the time domain. Relation between the maximum value of delay spread and channel coherence time is inversely proportional. Delay spread has similar effect on received signal in time domain as the Doppler spread in frequency domain. Due to Doppler phenomenon the received signal is spread in frequency domain while delay spread introduces time dispersion for received signal. Hence, time dispersion refers to multiple copies of transmitted signal with significant energy and spread over the time domain, Figure 12.

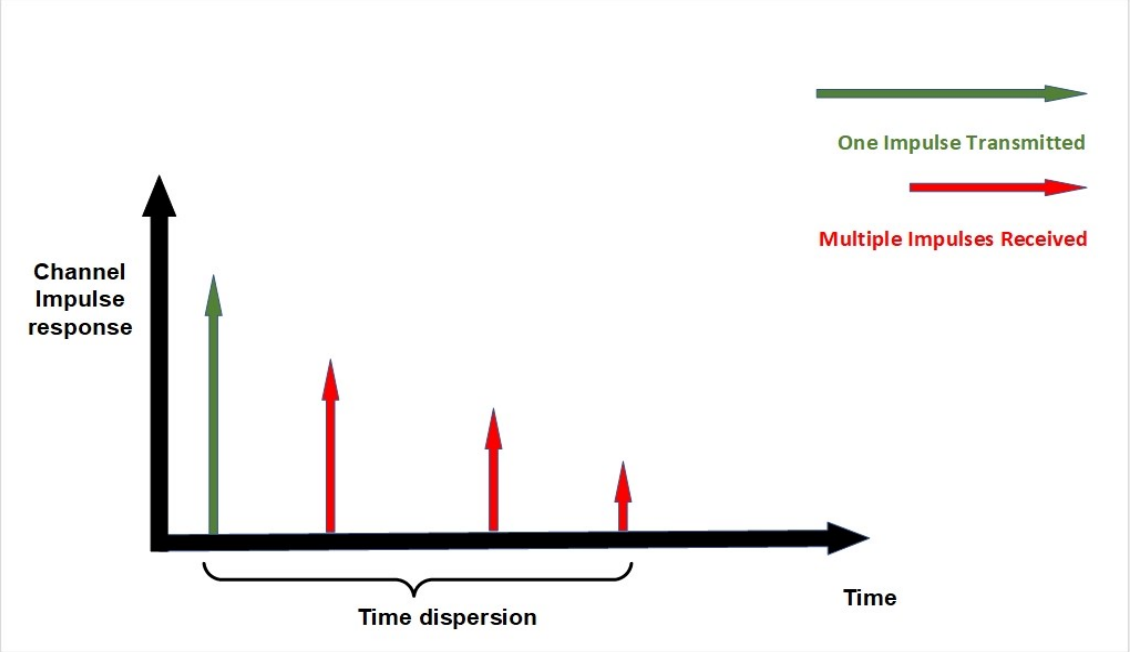

Figure 12. *Time dispersion as delay spread resultant*

Besides, the channel impulse response becomes a cascade of different multipath impulses with varying energy level received at different time instances. Moreover, RMS

delay spread is described as the root-mean-square value or standard deviation of reflection delays weighted proportional to energy of reflected waves in various multipaths. In the table below, typical outdoor and indoor RMS delay spread values [12] are given. The RMS delay spread values given in Table 1 are obtained from various case studies mentioned in separate source-column in the Table below.

Table 1. Typical RMS Delay spread in various environments

Environment	Frequency (MHZ)	RMS Delay spread (ns)	Notes	Source
Indoor – Office building	1500	10-50		[13]
Indoor – Office building	1500	25	Median	[13]
Indoor – Office building	850	270	Maximum	[14]
Indoor – Office building	1900	70-94	Average	[15]
Indoor – Office building	1900	1470	Maximum	[15]
Urban – New York city	910	1300	Average	[16]
Urban – New York city	910	600	Standard deviation	[16]
Urban – New York city	910	3500	Maximum	[16]
Urban – San Francisco	892	1000-2500	Worst case	[17]
Suburban	910	200-310	Averaged typical case	[16]
Suburban	910	1960-2110	Averaged extreme case	[16]

From ***Table 1***, it can be observed that RMS delay spread is proportional to the area of propagation. Considering indoor environments, multipath delays are smaller as a resultant of smaller propagation area whereas, in outdoor environment multipath delays are larger due to larger propagation area. Moreover, reflector components such as walls regarding indoor environment are in close vicinity with the receiver whereas, in outdoor environment reflector component such as large buildings or trees are not as close to receiver as indoor environment.

2.4 Channel coherence bandwidth and coherence time

Channel coherence bandwidth can be defined as the bandwidth or range of frequencies over which the channel is constant i.e. minimal signal attenuation over the channel. Coherence bandwidth can be effectively calculated through RMS delay spread [18].

$$Coherence\ bandwidth \approx \frac{1}{2\pi * RMS\ Delay\ Spread} \tag{2.20}$$

However, in practical scenario, 50% coherence bandwidth is more frequently used.

$$Coherence\ bandwidth_{50\%} \approx \frac{1}{5 * RMS\ Delay\ Spread} \tag{2.21}$$

The 50% coherence bandwidth depicts that, two frequencies separated by $Coherence\ bandwidth_{50\%}$ have 0.5 correlation [5].

Coherence bandwidth is not much affected by mobility to some extent. As seen in the equation, coherence bandwidth is only dependent on RMS delay spread and the delay spread is a resultant of multipath. In the context of local area network environments, the delay from various path is limited because of the concise area between transmitter and receiver themselves. As a result, the average delays from different multipaths are seldom higher. Besides, the Doppler is relatively small because these environments support smaller mobility. Moreover, the delay spread not being a direct function of speed or mobility is less affected by the vehicle speed.

Coherence time can be defined as the time span over which the channel is constant or nearly constant [18].

$$coherence\ time = \frac{1}{2\pi * f_{max}} \tag{2.22}$$

Here,

$$f_{max} = \frac{vehicle\ speed}{\lambda_{carrier}} \tag{2.23}$$

$$\lambda_{carrier} = \frac{c}{f_{carrier}} \tag{2.24}$$

Again, in practical scenario, 50% coherence time is more frequently used.

$$coherence\ time_{50\%} = \frac{9}{16\pi * f_{max}} \tag{2.25}$$

The 50% coherence bandwidth depicts that, two channel outputs separated by $coherence\ time_{50\%}$ have 0.5 correlation [5].

Coherence time is greatly affected by mobility as from equations above, the parameter f_{max} is a direct function of vehicle speed as well as mobility. Coherence time can be described as the parameter that needs to get updated more frequently for the channel information with increased mobility. Mentioned phenomenon is illustrated in Figure 13,

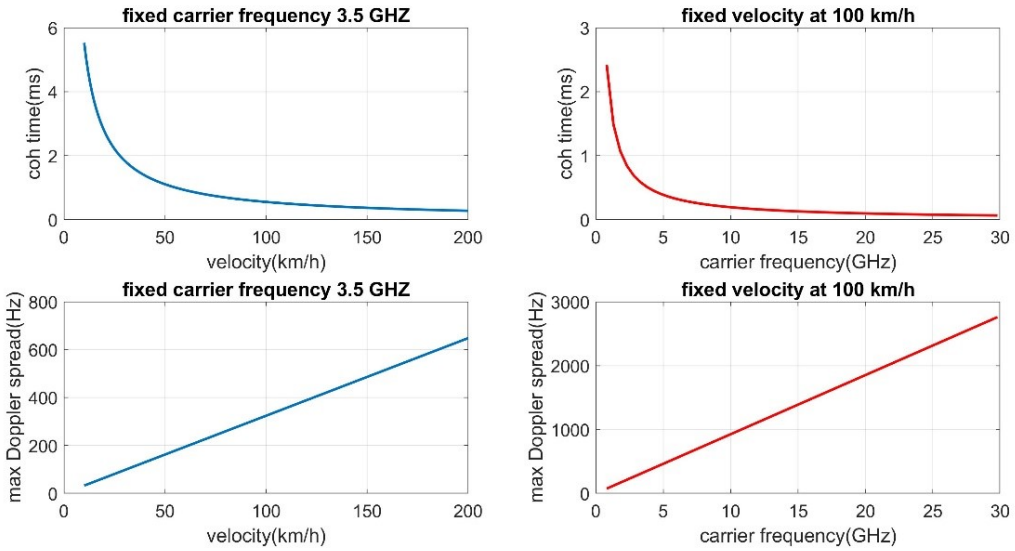

Figure 13. *Effect of velocity (ranging from 10 to 200 km/h) increase on coherence time and maximum Doppler spread (left sided figures)when carrier frequency fixed at 3.5 GHz ; effect of carrier frequency (ranging from 800 MHz to 30 GHz)increase on coherence time and maximum Doppler spread (right sided figures) when velocity fixed at 100 km/h*

The above figure is a test case scenario for 50% coherence time, i.e. the correlation in time domain between two delayed channels is more than 0.5. As illustrated in Figure 13, coherence time is comparatively smaller for higher velocity resulting in frequent need for time updates for concerned channel. Channel outputs become less correlated with higher velocity as well as higher maximum Doppler spread values. With increasing carrier frequency, the phenomenon converges similarly.

In the context of scheduling channel resources, coherence time plays a vital role as the coherence time measurement must be considered. Besides, the validity of coherence time is significant as the scheduling of channel resources depends on whether the time measurements are valid, or it needs to get updated again.

2.5 MIMO Aspects

MIMO stands for multiple input multiple output used in both transmitter and receiver end. The technique is used for better channel quality, channel capacity and coverage in capacity controlled networks. Moreover, MIMO turns the disadvantage of multi-path propagation into advantage by exploiting multi-path rather than mitigating it [19]. In this methodology multiple antennas are used in transmitter to send numerous parallel signals. Besides, at the receiver end signal processing is opted for producing the transmitted signal from these parallel signals travelling in multi-path. The main advantage of MIMO is that multiple streams of data can be transmitted over a single channel simultaneously.

Thus, the phenomenon results in increased capacity, coverage and data throughput. For example, regarding a 4x4 MIMO, the throughput can be four times as four copies of data stream can be sent over the same channel simultaneously. Besides, the MIMO methodology is adopted for aiding multipath fading as well as thermal noises. The receiver antenna receives signals from adjacent propagation paths besides the intended signal. Hence, the MIMO channel response can be illustrated as transmission matrix ***H***,

$$b = \boldsymbol{H}a + n \tag{2.26}$$

where, *b* is receiver antenna output vector, *a* is transmitter antenna input vector and *n* is the noise vector.

The transmission matrix, ***H*** can be described as follows,

$$\boldsymbol{H} = \begin{bmatrix} h_{11} & h_{12} & \dots & h_{1a} \\ h_{21} & h_{22} & \dots & h_{2a} \\ \vdots & \vdots & \vdots & \vdots \\ h_{b1} & h_{b2} & \dots & h_{ba} \end{bmatrix} \tag{2.27}$$

where, h_{11}, h_{12}, h_{21}, h_{ba} are defined as various transmission paths. The various transmission paths are illustrated in Figure 14.

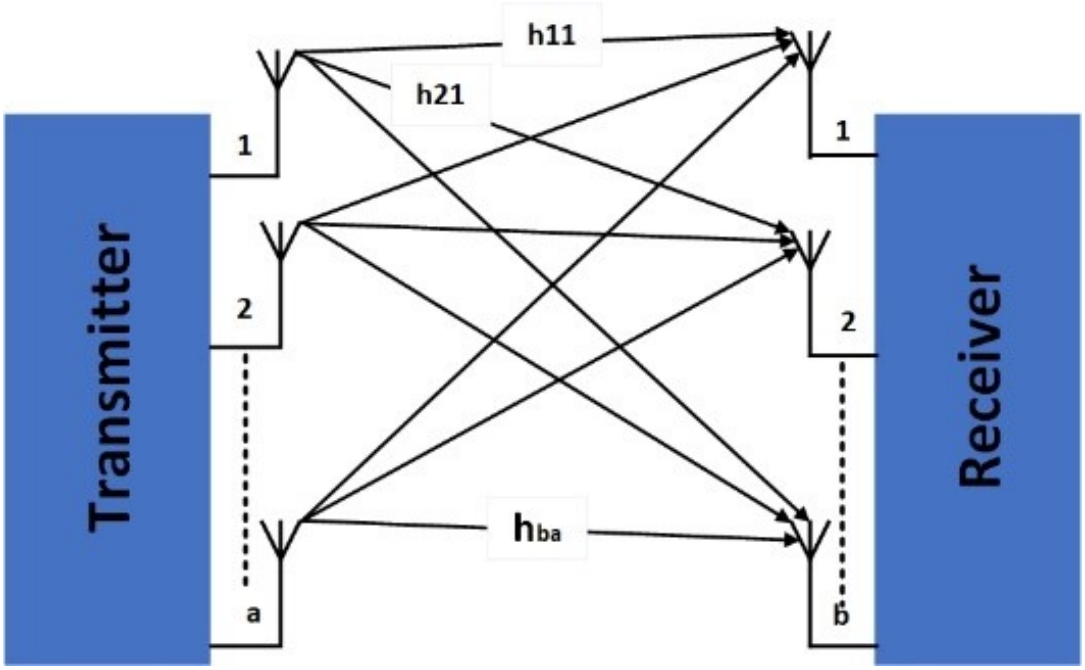

Figure 14. *A general outline of MIMO system, transmission matrix* ***H*** *is formed considering various transmission paths like h11, h21,* h_{ba} *etc.*

However, regarding mobility of the transceivers the MIMO scenario becomes complicated. Firstly, motions of transceivers bring changes to channel matrix. Besides, condition number of $\boldsymbol{H}$ becomes high due to mobility as there will be more paths introduced [19]. The high condition number makes it very difficult for the receiver to solve the set of

linear equations making the system ambiguous and unstable as well as affects the multiplexing ability in a MIMO link. Thus, lower condition number of matrix ***H*** makes the multiplexing more reliable. Moreover, rank of matrix ***H*** defines number of data streams that can be multiplexed in a link. Finally, regarding mobility the matrix ***H*** requires better estimation for reliable channel conditions [19].

2.6 cmWave (centimetre wave) vs. mmWave (millimetre wave) Channel

cmWave and mmWave channels are defined based on the wavelength of the frequency band used in the respective communication channel. cmWave is defined between the frequency band 6 GHz and 30 GHz with better data rates, precision in geolocation and ranging. Noticeably, available cmWave spectrum between 6 GHz and 28 GHz is approximately 2.5 GHz [20]. On the other hand, mmWave is defined as frequency band ranging beyond 30 GHz. Besides, non-occupied spectrum scopes in mmWave context are comparatively larger than cmWave, for example, approximately 4 GHz in the range of 38 GHz, 10 GHz in the range between 70 GHz and 86 GHz as well as 3 GHz in the range of 90 GHz [20]. In Figure 15, the scenario is illustrated in the context of usage and sharing scheme.

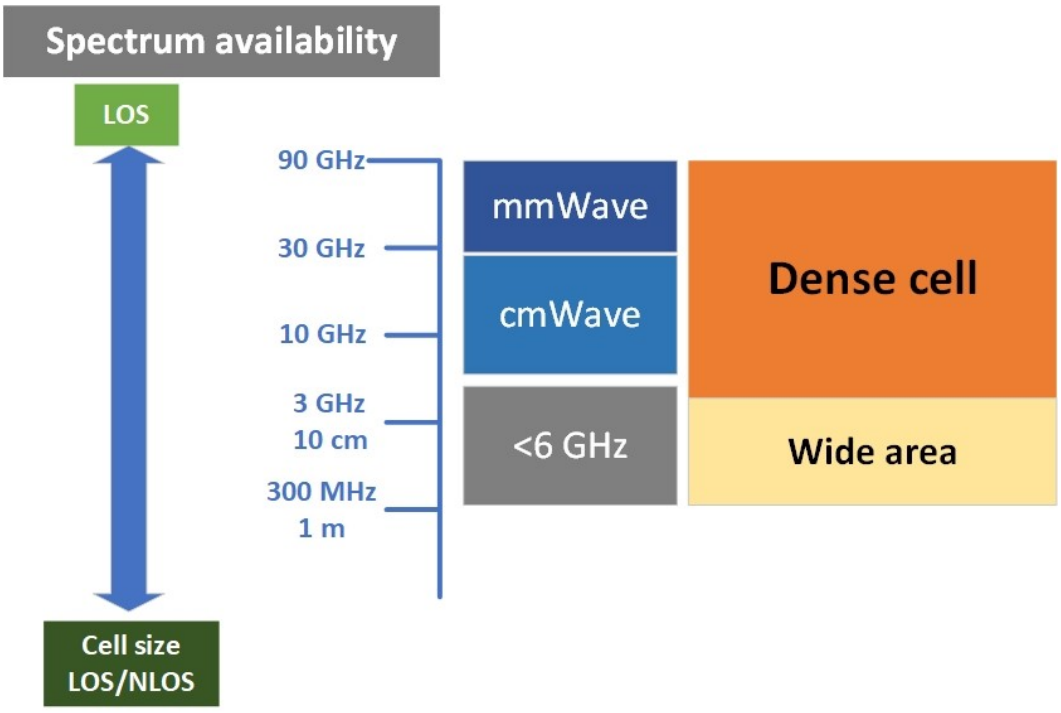

Figure 15. *Different spectrum licensing, usage and sharing schemes*

With increasing demand for bandwidth as well as over-crowding in ultra-wideband, commercial application use of the unlicensed frequency band of 60 GHz is in mainstream focus because of the possibility of providing higher data rates, reduction in system interference as well as in frequency reuse distance [21]. Martinez Ingles *et al.* (2014) an experiment mentioned in the study [22], argues that the path loss in an indoor environment regarding LOS (line of sight) is higher for mmWave than cmWave channel. Besides, considering RMS delay spread, mmWave channel has shorter RMS delay spread as well as shorter transmit time interval (TTI) than cmWave channel. Moreover, considering LOS, multi-path components in mmWave channel are less significant due to shorter delay spread and higher electrical distances for decorrelation whereas multi-path components play a vital role in cmWave channels. However, considering mobility, Doppler effect is higher in mmWave channel as a result of magnitude of Doppler effect being proportional to the used carrier frequency [22]. Finally, the current cellular networks work at cmWave and sub 6 GHz, whereas mmWave are considered to be compatible with current cellular networks in the near future.

3. MOBILITY MODELS FOR DIFFERENT VEHICULAR COMMUNICATION SCENARIOS

In the modern era of communication with increasing vehicle connectivity requirements, it is of great significance to define vehicle movement models and consider the radio channel parameters accordingly. Therefore, speculation should be done for radio channel parameters such as Doppler effect, delay spread, coherence time and bandwidth along with multiple input multiple output (MIMO) aspects regarding user equipment (mobile phones or radio units) inside or mounted on the vehicle of each type. To understand designing of communication links, different performance aspects such as throughput, latency, reliability and availability, it is important to know the speed and position of the user equipment with respect to the base station. The mobility models can work as the algorithm to achieve the speed and position of user equipment. For the car mobility model Akcelik and Biggs polynomial model [23] is considered, whereas for trains and UAVs, EIM (element increment method) [24] and Gauss-Markov random mobility models [25] are considered.

3.1 Car Mobility Models

Acceleration and deceleration profiles are the starting point to define the behaviour of cars. Cars in traffic accelerate, decelerate or come to a complete stop depending on the behaviour of other vehicles, traffic signals, bending of the road, lane changing or any hazardous circumstance. Cars have limitations to speed variations and sudden position changes because of mass and controlled traffic scenarios. For example, a car must follow other cars in traffic as well as extremely sudden position changes are seldom possible because the mass of the car. Besides, while taking turns the variation of speed can be speculated from the curvature of the bend and turning speed. A polynomial model [23] developed by Akcelik and Biggs is considered the most simplistic reliable model based on the simulation outputs and comparison between two other models; namely, a two-term and three-term sinusoidal model. The polynomial model is best suited for traffic as it is based on a large pool of real-life traffic data collected by mechanical department of Sydney University from urban, sub-urban and rural roads. Furthermore, the convergence between the simulation results and basic laws of physics defines the reliability of the model chosen. The model output is defined as three parameters: acceleration or deceleration rate, speed and distance travelled. Besides, Doppler shift and delay spread

can be observed as a resultant of position and distance of user equipment. The observation of speed and detailed analysis of position calculation can give an overview of the effects on radio channel parameters and designing aspects regarding communication link. The polynomial function developed[23] for estimating rate of acceleration at a given time t,

$$A(t) = Ra_m\theta^n(1-\theta^m)^2 \quad (n > 0, m > -0.5n) \tag{3.1}$$

where, $A(t)$ is the rate of acceleration at time t, a_m is the maximum acceleration, θ is time ratio (t/t_a), t is time since the acceleration started, t_a is total time to achieve the final speed, m, n = deterministic parameters, R is m, n value dependent parameter and given by,

$$R = \left[(1+2m)^{2+1/m}\right]/4m^2 \tag{3.2}$$

Values of m, n are chosen in such a manner that the above function in equation (3.1) represents various acceleration profiles. A simplistic approach to determine the values of m, n is to set n to be constant and then choose the value of m. For practical use a simpler model with n = 1 is as follows,

$$A(t) = Ra_m\theta(1-\theta^m)^2 \quad (m > -0.5n) \tag{3.3}$$

Another link to design various acceleration profiles is speed ratio ρ, that defines the ratio between average speed in acceleration and final speed, $\rho = V_a / V_f$, assuming initial speed (V_i) to be zero.

Relation between the above polynomial model in equation (2) and deterministic speed at time t or time stamp dx/dt can be given as,

$$V(t) = V_i + t_a r a_m \theta^2 \left[0.5 - \frac{2\theta^m}{m+2} + \frac{\theta^{2m}}{2m+2}\right] \tag{3.4}$$

Besides, deterministic distance at time t or time stamp dx/dt can be given as,

$$L(t) = \frac{V_i\, t}{3.6} + R\; a_m t_{a/d}^2\; \theta^3 \left[\frac{1}{6} - 2\frac{\theta^m}{(m+2)(m+3)} + \frac{\theta^{2m}}{(2m+2)(2m+3)}\right] \tag{3.5}$$

Finally, the acceleration and deceleration profile can be achieved even if the acceleration time, acceleration distance, deceleration time and/or deceleration distance are unknown.

Based on Sydney data the regression equations for acceleration time (t_a) and acceleration distance (X_a) for acceleration profile are given as,

$$t_a = \frac{V_f - V_i}{2.08 + 0.127\left(V_f - V_i\right)^{\frac{1}{2}} - 0.0182V_i} \tag{3.6}$$

$$X_a = \frac{\left(0.467 + 0.0020V_f - 0.0021V_i\right)\left(V_i + V_f\right)t_a}{3.6} \tag{3.7}$$

Regression equations for deceleration time (t_d) and deceleration distance (X_d) for deceleration profile are given as,

$$t_d = \frac{V_i - V_f}{1.71 + 0.238\left(V_i - V_f\right)^{\frac{1}{2}} - 0.0090V_f} \tag{3.8}$$

$$X_d = \frac{\left(0.473 + 0.00155V_i - 0.00137V_f\right)\left(V_i + V_f\right)t_d}{3.6} \tag{3.9}$$

The algorithm presented above, including Equations 3.1-3.8, determines acceleration as well as deceleration profile for a car moving independent of parameters such as traffic scenario, bending of the road and lane changing behaviour. Besides, the algorithm provides acceleration rate, deceleration rate, velocity and distance accordingly. Moreover, in Figure 16, acceleration and deceleration profile is shown for a car having a maximum speed of 100 km/h and minimum speed of zero.

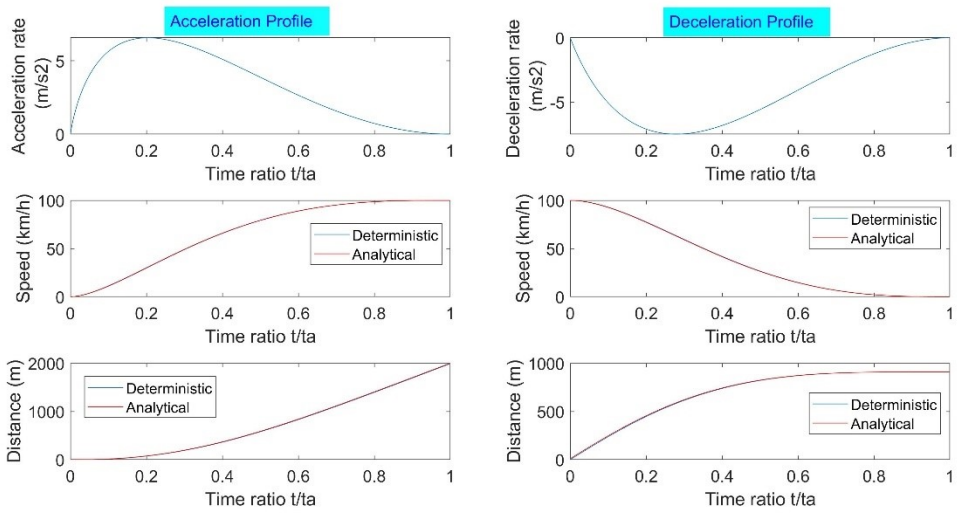

Figure 16. *Acceleration and deceleration profile achieved from Polynomial model [1]*

As seen in Figure 16, deterministic curve is achieved from simulating the previous mentioned algorithm for acceleration as well as deceleration scenario whereas, the analytical curve is achieved from simulating the same scenario according to the basic laws of physics such as, Newton's law of velocity and distance i.e. integrating acceleration to get velocity and integrating velocity to get distance. Moreover, in Figure 16, both analytical and deterministic curve converges adroitly. Based on the polynomial model [23] discussed, another model [26] is developed for cars turning in curves and following car behaviour in traffic by Carillo Gonzalez et al. (2014). Carillo proposes safety distance

parameters should be defined between first and following vehicles. For defining safety distance parameters two models have been proposed [26]: parameter estimator and double sigmoid. The first model describes the behaviour of cars based on the speed, acceleration, safety distance and reaction time, whereas the double sigmoid model tries to extrapolate the speed of a leader vehicle by utilizing four samples in a third order polynomial equation to project the distance between the vehicles in the calculus equation regarding the double sigmoid model algorithm. Besides, a behavioural pattern of the vehicle entering a curve is described by dependent variables (heading angle and speed) and independent variables (time and the coordinates of vehicle position) [26] . The heading angle of a vehicle in curves is described by the coordinates (3D-coordinates) of the vehicle position. However, as the vehicle has no movement in the axis normal to plane (typically z-axis), only x and y axis are considered in the final explanatory equation.

3.2 Train (high speed) Mobility Models

Train mobility models are simpler than the car mobility models as movement for trains are comparatively more restricted. Trains are built to follow tracks where the degree of free movement is more limited. As the acceleration and deceleration mechanism work in a complicated way, the train speed simulation can be done in element increment method developed by Xu et al, (2016) where the distance between the starting point and the end point is divided into several elements depending on the regulation of switching operation modes: pulling, coasting or breaking. In element increment method scenario the train track is considered as segments rather than a continuous line. Position and velocity solution regarding each element are calculated considering the adjacent elements. In this simulation approach train velocity variance is calculated by time increment method with the aid of polynomial fitting and later step-by-step integration method is used for combining the elements to make the simulation curve continuous [24]. However, an approach for developing a cellular Automaton model for the simulation of train trajectory, factors like geometry of railroad, traction of equipment as well as train length have not been considered [27].

Position and velocity solution for trains is achieved from train dynamic calculation [28]. However, in the train dynamic calculation scenario, net force calculation is of great significance. The net force of a train is composed of three basic forces, namely, force of powering or breaking, force of resistance and additional resistant force. Moreover, the net force is of varying in nature with the change in velocity as the acceleration working behind powering or braking force is not constant in nature. Hence, a common approach to simplify the varying nature of net force is to assume it to be constant over a short

distance. Moreover, the mass of train is considered to be a single particle which simplifies the computational load but decreases the accuracy aspects. Therefore, an iterative approach adopted to interrelate the adjacent elements. In this iterative approach the simulation curve of discrete elements is conjoined together based on entering and departure velocity of each element. Besides, the departure velocity of the former element is considered as the entering velocity of the current element. In case of deceleration in a current element the departure velocity of the previous element should not be higher than the maximum speed of current element to avoid overspeed. Therefore, length of the current element is considered to calculate a new entering velocity for the current element that replaces the previous entering velocity or the departure velocity of former element. Nevertheless, while calculating a current element it is seldom possible to simultaneously consider the influence on adjacent elements. Finally, the iteration ends when there is no replacement from first element to the last element [24]. The formula for calculating the net force regarding a train is as follows,

$$C = \frac{(Fy - W - B) \times 10^3}{M.g} \tag{3.10}$$

where, *Fy* is force of traction, *W* is force of resistance, *B* is force of braking, *M* is total train mass and *g* is the gravitational acceleration. Besides, acceleration and velocity increment can be represented by,

$$a = \frac{g}{1060}\, C \tag{3.11}$$

$$\Delta v = a\Delta t \tag{3.12}$$

From the model algorithm presented above, including equation 3.10-3.12, simulation of velocity, net force and distance is conducted. Noticeably, force of braking *B* is assumed zero for simplicity considering acceleration as well as cruising speed simulation scenario. However, considering deceleration baking force is needed to make the train stop. Moreover, force of traction *Fy* as well as force of resistance *W* is formulated [24] according to the following equations,

$$F_y = \begin{cases} 176 - 0.36v, & \text{and} 0 \le x \le 125 \;\; km/h \\ x, & \text{and} x > 125 \;\; km/h \end{cases} \tag{3.13}$$

where, unit for *Fy* is in kN.

$$W = 8.63 + 0.07295v + 0.00112v^2 \tag{3.14}$$

where, unit for v is km/h and unit for *W* is in N/t. From, equation 3.13 and 3.14, with

increasing velocity the net force working on a train decreases as shown is Figure 17. Moreover, the maximum net force works at zero initial velocity to achieve the maximum speed. Finally, net force decreases as the train reaches maximum constant coasting velocity.

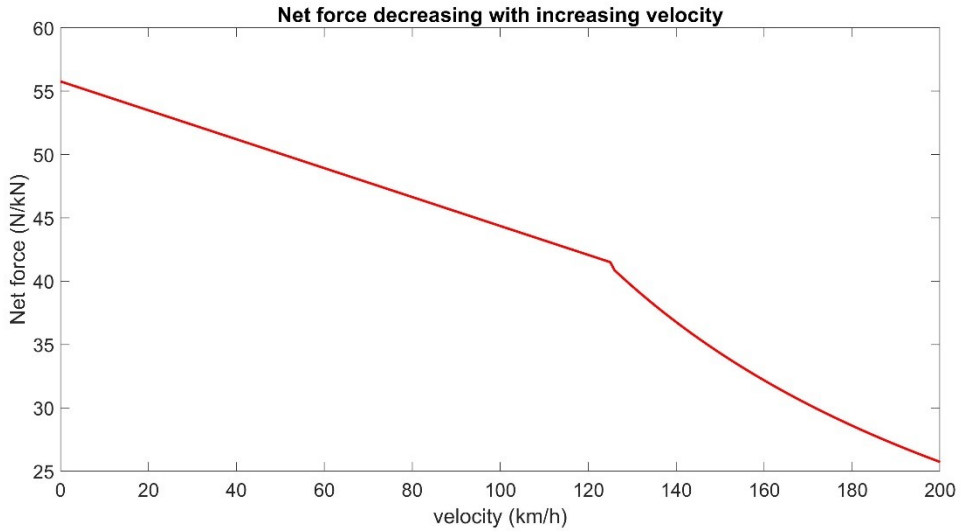

Figure 17. *Net force vs velocity*

From algorithm simulation, in Figure 18, distance covered to reach the maximum velocity is shown. Moreover, the distance is calculated as a function of velocity assuming zero initial distance. The distance achieved from the simulation is used as the position in single direction in the Kalman filter position estimates later.

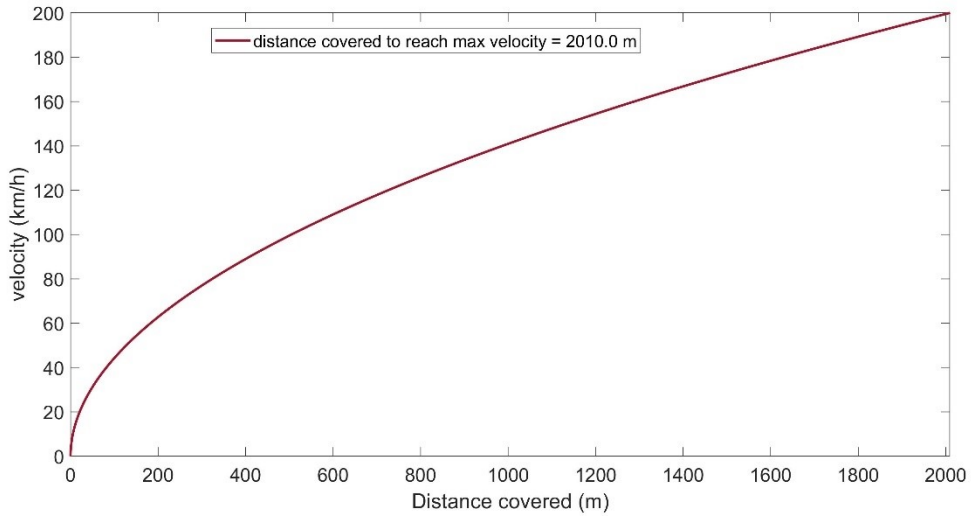

Figure 18. *Velocity vs distance covered to reach maximum velocity*

Finally, the velocity-time curve for train mobility model simulation is presented in Figure 19. From the algorithm simulation, a Talgo 350 train weighing 322 Tons [29] takes approximately 233.6 seconds or roughly 4 minutes to reach a maximum velocity of 200 km/h.

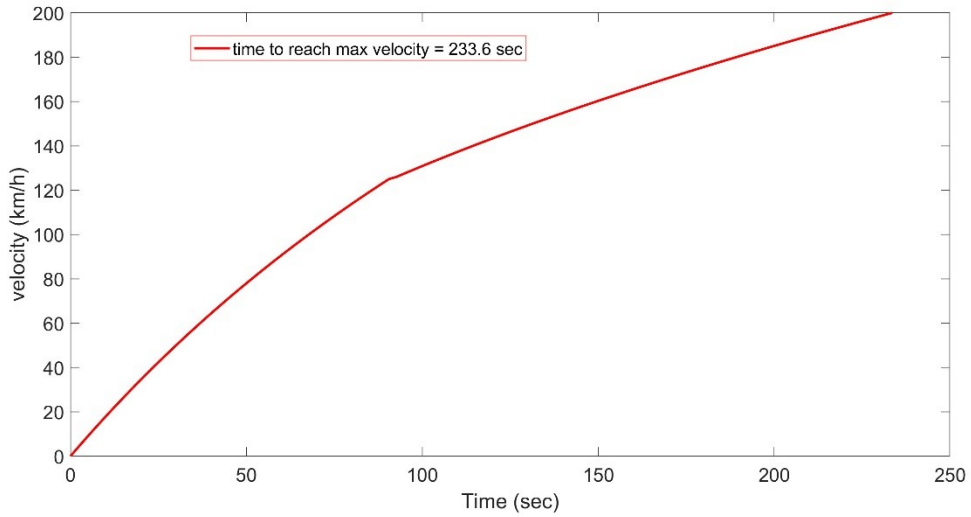

Figure 19. *Velocity vs time curve considering train mobility scenario*

3.3 Drones/UAV (airborne network) Mobility Models

With the increasing air traffic, need for random UAVs mobility model is on the rise to evaluate the networking performance. The mobility models are considered fundamental in airborne network design and analysis aspects due to the importance of safe manoeuvring, information sharing in real time and successful coordination [30]. Selecting effective mobility model for airborne networks is difficult compared to low mobility ground networks due to higher mobility and dynamic topology [31]. Mobility of aerial vehicles stands apart from ground vehicles due to aerodynamic constraint. Among the five main categories of mobility models [32], [33], including pure random models, models with temporal dependency, models with spatial dependency, models with geographic dependency and hybrid models, the first two categories are considered according to thesis scope. Furthermore, pure random models can be classified into three other models regarding the nature of randomness, namely, Random Walk Model (RW), Random Waypoint Model (RWP) and Random Direction Model (RD) [34]-[36]. Random walk model gives aerial trajectory the liberty to choose the heading direction and speed for a fixed period [37]. Besides, Random waypoint model gives liberty to choose the destination and speed in a region but with a restriction considering region boundaries which pushes node locations towards the region centrum [38]. The Random direction model gives liberty to choose speed, heading destination and duration whereas for exponential distribution mean of

travel duration becomes variable [39]. Even though this mentioned pure random models can capture high mobility, a major downside is uncorrelated heading variable. Due to this uncorrelated heading variable, correlation regarding movement becomes unknown across space-time dimension resulting in unpredicted directional changes. Moreover, in the context of non-smooth trajectories, these random models are considered abstract for being memoryless, i.e. time slot selection is random as well as uncorrelated [30].

For resolving the uncorrelated time slot phenomenon, memory-based Gauss-Markov Random Mobility model can aid with temporal correlation property [40], [41]. The temporal correlation is resultant of continuous time dynamics of Gauss-Markov model [42] that can be represented as,

$$\dot{P}(t) = -B\,P(t) + BPavg + \sqrt{2B}\sigma N(t) \tag{3.15}$$

Where, *P(t)* is state variable, *σ* is constant value, *N(t)* describes the white Gaussian noise with zero mean and unity variance, *B* describes the correlation of state variable in time, *Pavg* is average of *P(t)* in steady state. Equation (3.15) is a representation of white Gaussian noise in a linear system. Moreover, the state variable vector can represent either velocity in x and y axis or the heading speed and heading direction considering a two-dimensional simulation scenario. Main property of Gauss-Markov model is memory of motion derived from autocorrelation of state variable in continuous time dynamics state. Now, defining $\tilde{P}(t) = P(t) - Pavg$, and $\widetilde{N}(t) = \sqrt{2B}\sigma N(t)$, from autocorrelation property of Gaussian process,

$$C_{\widetilde{P}\widetilde{P}}(\tau) = E\left(\widetilde{N}(t+\tau)\widetilde{N}^{*}(t)\right) = 2B\sigma^{2}\delta(\tau) \tag{3.16}$$

Besides, defining $S_{\widetilde{N}\widetilde{N}}(\omega) = 2B\sigma^{2}$, power spectrum can be described as,

$$S_{\widetilde{P}\widetilde{P}}(\omega) = S_{\widetilde{N}\widetilde{N}}(\omega)H(\omega)H^{*}(\omega) = 2B\sigma^{2}\frac{1}{(i\omega - B)}\frac{1}{(-i\omega - b)} = \frac{2B\sigma^{2}}{\omega^{2} + B^{2}} \tag{3.17}$$

Therefore, the autocorrelation of state variable regarding steady state [43] ,

$$R_{PP}(\tau) = \sigma^{2}e^{-B|\tau|} + Pavg^{2} \tag{3.18}$$

From equation (3.18), correlation of state variable decreases in an exponential manner with increase in time interval τ. Hence, motion changes are more correlated with larger time interval.

A discrete time representation of equation (3.15), τ becomes sampling time Δt [43] ,

$$P[k+1] = AP[k] + (1-A)Pavg + \sqrt{2B}\sigma\int_{k\Delta t}^{(k+1)\Delta t} e^{-B\Delta t}N(t) \tag{3.19}$$

When, k proceeds to infinity, the integral part of equation (3.19) represents Gaussian process with zero mean and variance, $\sigma^{2} = 1 - e^{2B\Delta t}$. Rewriting equation (3.19),

$$P[k+1] = AP[k] + (1-A)Pavg + \sqrt{1-A^2}\sigma G[k] \tag{3.20}$$

where, *G[k]* represents independent Gaussian process with zero mean and unity variance.

Furthermore, Gauss-Markov model consists of four main parameters, level of independence *A*, average *Pavg*, Gaussian noise variance $\boldsymbol{\sigma}$ and simulation time stamp Δt. Parameter for level of independence, *A* can be described as correlation parameter as well. With the increase of *A,* the correlation regarding motion among consecutive time stamps increases. Increase in correlation means drastic and sharp motion changes can be avoided [44]. The correlation parameter is also directly related to memory of the Gauss-Markov model. When, *A*=0, there resides no memory of the system as the states are now completely uncorrelated and *A* being one represents the system to be free of motion changes over time. Moreover, with higher *A*, the trajectories become straighter as variation decreases. The Gauss-Markov model is more realistic in the context of aerodynamic constraint capturing than the pure random models as real-life aerial vehicles are prone to straight trajectories and soft turns. In Figure 20, a comparative overview of correlation parameter *A* is shown,

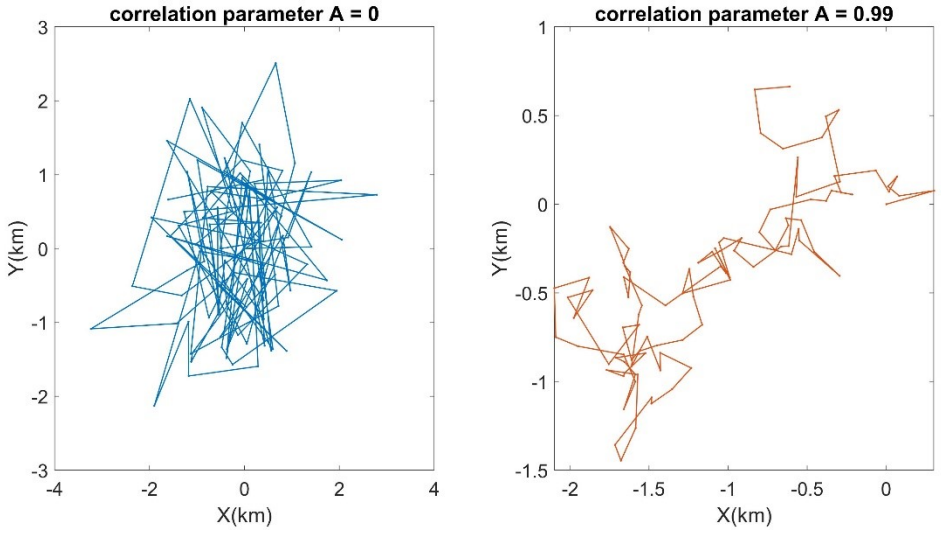

Figure 20. *Comparative overview of two different valued correlation parameter A*

From Figure 20, zero valued correlation parameter represents null correlation between consecutive data points, whereas, *A*=0.99 refers to high correlation between consecutive data points. Furthermore, the high correlation results in less random position data as well as soft turn phenomenon can be observed likewise. However, zero correlation represents a memory less system resulting in hard and random turns as well as uncorrelated random position data. Noticeably, in the simulation a hundred iterative loop is considered

for taking a hundred data point from Gauss-Markov model. Moreover, the overall scenario becomes more transparent in Figure 21, where cumulative summation method for the data points is adopted. Finally, greater correlation value results in more smooth and straighter trajectories in UAV position modelling scenario.

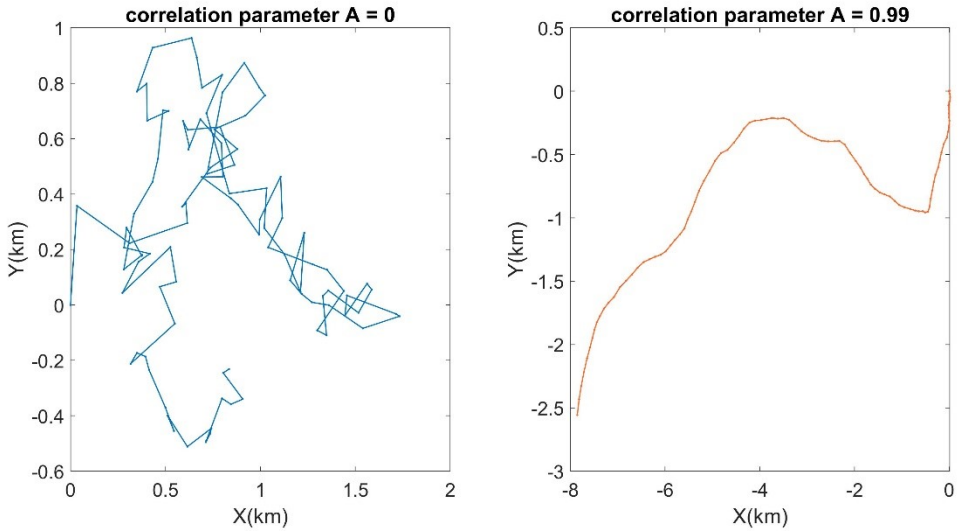

Figure 21. *Cumulative method for data points*

3.4 Pedestrian Mobility Models

As a part of whole mobility model scenario in a simulation environment, pedestrian mobility model is discussed in this subsection in a comparative overview. In context with degree of freedom related to object movement scenario, pedestrian model is quite random compared to vehicular movement. Cars following the behavioural pattern of other cars in traffic have limited degree of freedom whereas the pedestrian movement is comparatively random and relatively free of traffic restrictions. Besides, mobility for high speed train is more restricted and concisely directional due to train tracks and momentum. However, in the context of unmanned aerial vehicles or drones, the mobility is not only limited to horizontal axis, but also vertical movement must be taken into consideration. As discussed in previous subsection, the memory based UAV movement model compensates for the random behaviour of movement. Besides, pedestrian movement differs from sidewalk to busy intersection in traffic [45]. However, due to slower speed, effect of pedestrian mobility on channel parameters such as Doppler effect is low.

4. UTILIZING MOBILITY MODELS FOR POSITIONING AND TRACKING

The discussed mobility models work as a reference for estimating the positioning and tracking in context of vehicular and pedestrian movement scenario. The mobility models basically give an estimation about velocity, acceleration and time reference regarding the subject of interest. However, in positioning and tracking scenario, need for definite futuristic estimation results in adopting filtering methodologies. The filtering approach aids for tracking user position from a mobility model through estimating variables in noisy and uncertain measurements.

4.1 Kalman Filter Methodology

Kalman filter is considered as an estimation technique preferably than a filter, developed by R.E. Kalman in 1960. This Bayesian approach for estimation technique is one of the popular methodologies for estimating future states in a continuous-time system. Firstly, some priori estimates about system parameters is provided to the Kalman filter. Then, through recursive operation, the filter decides the working estimates using knowledge regarding the properties of system parameters as a weighted average of priori and new estimates from recently measured data. This recursive process is more processor friendly in the sense that only new measurement data in each iteration loop need to be processed rather than the whole data stream [46].

The Kalman filter methodology consists of five key elements, namely, state vector, system model, measurement vector, measurement model and algorithm. Besides, state vector and measurement vector are associated with covariance matrix where the uncertainties regarding estimates as well as error correlation is considered. Moreover, the system model represents the time varying nature of state vector and associated error covariance matrix. However, the measurement vector is associated with measurement error covariance matrix that describes the noise effect on measured data after initialization. Noticeably, the measurement model explains the varying nature of measurement vector based on true state vector when measurement noise is absent. Moreover, both system model as well as measurement model are deterministic if system properties are known. Finally, the algorithm decides optimal state vector estimates based on measurement vector, measurement and system model [46].

The Kalman filter methodology works on basis of feedback control considering time and measurement update. Besides, time update is considered a priori estimate whereas measurement update is considered a posteriori estimate. Kalman filter provides solution to estimate state $x \in \mathcal{R}^n$ of a process described by a difference equation,

$$x_k = Ax_{k-1} + Bu_{k-1} + w_{k-1} \tag{4.1}$$

Where, Ax_{k-1} is the state transition model, Bu_{k-1} is optional control unit and w_{k-1} is process noise $p(w) \sim N(0, \boldsymbol{Q})$, $\boldsymbol{Q}$ is denoted as process noise covariance. Moreover, x_k is the present state estimate dependent on the previous state estimate x_{k-1}, where A is a constant determining the relation between the two consecutive estimates.

State estimation is done through measurement $z \in \mathcal{R}^m$,

$$z_k = \boldsymbol{H}x_k + v_k \tag{4.2}$$

Here, Hx_k is observation model and v_k is the measurement noise. Hence, time update,

$$\hat{x}_k^- = A\hat{x}_{k-1} \tag{4.3}$$

$$\hat{P}_k^- = AP_{k-1}A^T + \boldsymbol{Q} \tag{4.4}$$

Therefore, measurement or observation noise covariance, $\boldsymbol{R}$ can be defined as $m(v) \sim N(0, \boldsymbol{R})$, where *N(.)* denotes multivariate normal distribution function.

Finally, measurement update,

$$K_k = P_k^- H^T (HP_k^- H^T + \boldsymbol{R})^{-1} \tag{4.5}$$

$$\hat{x}_k = \hat{x}_k^- + K_k(z_k - \boldsymbol{H}\hat{x}_k^-) \tag{4.6}$$

$$P_k = (I - K_k\boldsymbol{H})P_k^- \tag{4.7}$$

4.2 Applying Studied Mobility Models to the Kalman Filter Methodology

In this subsection velocity and position data achieved from mobility models is further modelled through Kalman filter methodology. For avoiding complexity, linear Kalman filtering approach is applied for processing the velocity and position data. However, the data for positioning is derived as a function of distance through velocity estimates for reducing complexity in simulation procedure. Moreover, the vehicle movement in x-axis is considered to have both accelerating and constant velocity states to analyse the Kalman filter outputs as a linear estimate. However, in the y-axis, vehicle movement is considered to have a constant position and zero velocity. Noticeably, heading of the vehicle remains constant during the simulation scenario. Finally, for modelling more accurate

simulation scenario Extended Kalman filtering approach can be adopted to handle non-linear parameters such as acceleration, angle or base-station coverage area.

In the context of simulation procedure for applying studied mobility models to the Kalman filter methodology, firstly, velocity and position data is achieved from the mobility model algorithm. The velocity and position data in both x-axis as well as y-axis is imported to Kalman filter in such a manner that the vehicle heading along both the axis remain constant i.e. the position and velocity along the x-axis is variable but the vehicle moves along the x-axis without any variation in the heading direction, whereas in the y-axis the vehicle position remains constant with zero velocity in y-axis direction.

Secondly, this velocity and position data is considered as true velocity and position. Furthermore, error is introduced to the true position data to achieve erroneous position measurements where the error introduced is Gaussian in nature. The procedure can be explained in a mathematical approach through following equations.

$$device\ absolute\ velocity = \sqrt{V_x^2 + V_y^2} \tag{4.8}$$

$$position\ mesaurement = \begin{bmatrix} P_x \\ P_y \end{bmatrix} + \frac{\sigma_{pos}}{\sqrt{2}} G_e \tag{4.9}$$

In equations 4.8 and 4.9, V_x, V_y are the velocity in x-axis and y-axis, P_x, P_y are the position in x-axis and y-axis, σ_{pos} is the standard deviation of position measurement error and G_e is the unit variance Gaussian noise vector of size 2x1 introduced to position measurements. Noticeably, the Gaussian error is scaled through σ_{pos}. Moreover, σ_{pos} defines the measurement covariance matrix that determines the measurement estimation accuracy. Therefore, lower value of σ_{pos} results in better position measurement. Besides, initial state vector, x_{k-1} consists of initial guess for position and velocity. Moreover, while deciding the initial guess for velocity Gaussian noise is introduced in the following manner,

$$Initial\ guess\ for\ velocity = \begin{bmatrix} V_{x0} \\ V_{y0} \end{bmatrix} + \frac{1}{\sqrt{2}} G_e \tag{4.10}$$

where, V_{x0}, V_{y0} are the first values of V_x, V_y, velocity data in x-axis and y-axis. Besides, initial guess for position measurement is achieved considering the first values of position measurement as described in equation 4.9. Besides, initial covariance, P_{k-1}, is defined as following,

$$P_{k-1} = \begin{bmatrix} \sigma_{pos}^2 & 0 & 0 & 0 \\ 0 & \sigma_{pos}^2 & 0 & 0 \\ 0 & 0 & \sigma_{pos}^2 & 0 \\ 0 & 0 & 0 & \sigma_{pos}^2 \end{bmatrix} \tag{4.11}$$

Size of P_{k-1} in equation (4.11) depends on the number of elements in initial state vector. Here, size of P_{k-1} is 4x4 as result of four elements in initial state vector, V_x, V_y, P_x and P_y.

Thirdly, another parameter for process covariance is sigma acceleration, σ_{acc}, that defines the oscillation of the estimated track. Noticeably, σ_{acc} should be changed according to the used mobility model. Besides, process covariance matrix, $\boldsymbol{Q}$ is defined by σ_{acc} in the following equation,

$$\boldsymbol{Q} = \sigma_{acc}^2 \begin{bmatrix} \frac{\Delta t^3}{3} & \frac{\Delta t^2}{2} \\ \frac{\Delta t^2}{2} & \Delta t \end{bmatrix} \otimes \begin{bmatrix} 1 & 0 \\ 0 & 1 \end{bmatrix} \tag{4.10}$$

Where $\otimes$ is defined as Kronecker tensor product between the two matrices, i.e. multiplying the second matrix by each element of the first matrix. Here, Δt is the time step duration for simulation. Besides, the state-transition matrix, $\boldsymbol{A}$ is defined as,

$$\boldsymbol{A} = \begin{bmatrix} 1 & \Delta t \\ 0 & 1 \end{bmatrix} \otimes \begin{bmatrix} 1 & 0 \\ 0 & 1 \end{bmatrix} \tag{4.11}$$

The measurement model matrix $\boldsymbol{H}$ can be described as following,

$$\boldsymbol{H} = \begin{bmatrix} 1 & 0 & 0 & 0 \\ 0 & 1 & 0 & 0 \end{bmatrix} \tag{4.12}$$

Besides, measurement or observation noise covariance, $\boldsymbol{R}$ can be defined as,

$$\boldsymbol{R} = E\left[v_k v_k^T\right] = \left[\sigma_{pos}^2\right] \tag{4.13}$$

4.2.1 Car mobility model analysis through Kalman filter

A car mobility model is designed from polynomial model [1], where the car has zero initial speed and a final speed of 100 km/h. Besides, the car covers a distance of 2000 m or 2 km to achieve the maximum constant speed of 100 km/h meanwhile. As mentioned before, the two dimensional position and velocity estimate approach takes the y-axis coordinate as a constant valued one regarding position. Finally, the car is moving along the x-axis with an acceleration period and constant velocity period as well as with a constant position and zero velocity in y-axis.

The most significant parameters effecting the simulation output is standard deviation of position measurement error, σ_{pos} as well as rate-of-change parameter regarding the state transition covariance, σ_{acc} in the Kalman filter. Firstly, the standard deviation for position measurement error, σ_{pos} defines the range for filtering out the position measurement to achieve the estimated track. As observed in Figure 22 and Figure 23, lower σ_{pos} value results in greater accuracy.

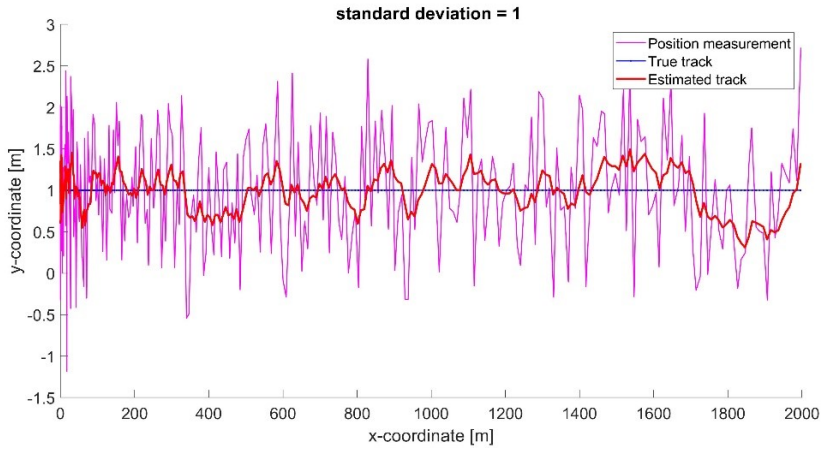

Figure 22. *Estimated position track for low σ_{pos}, σ_{pos}=1, σ_{acc}=0.5*

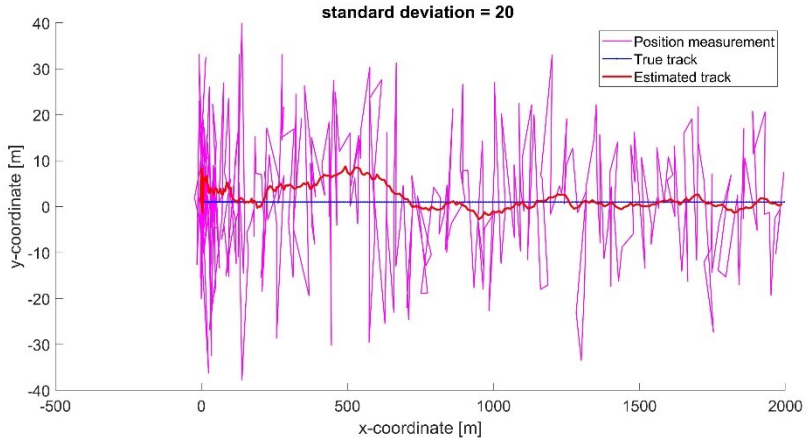

Figure 23. *Estimated position track for high σ_{pos}, σ_{pos}=20, σ_{acc}=0.5*

Noticeably, Figure 22 depicts a very good accuracy in position tracking as the filtering range is limited through standard deviation, σ_{pos} valued one.

Secondly, parameter σ_{acc} defining the process covariance $\boldsymbol{Q}$ is tuned to model the acceleration of the vehicle. Larger values of sigma acceleration results in more accurate velocity estimation. Besides, with increasing σ_{acc} position estimation accuracy degrades. However, the mentioned phenomenon depends on the underlying mobility model. Finally, the phenomenon is illustrated in Figure 24 and 25.

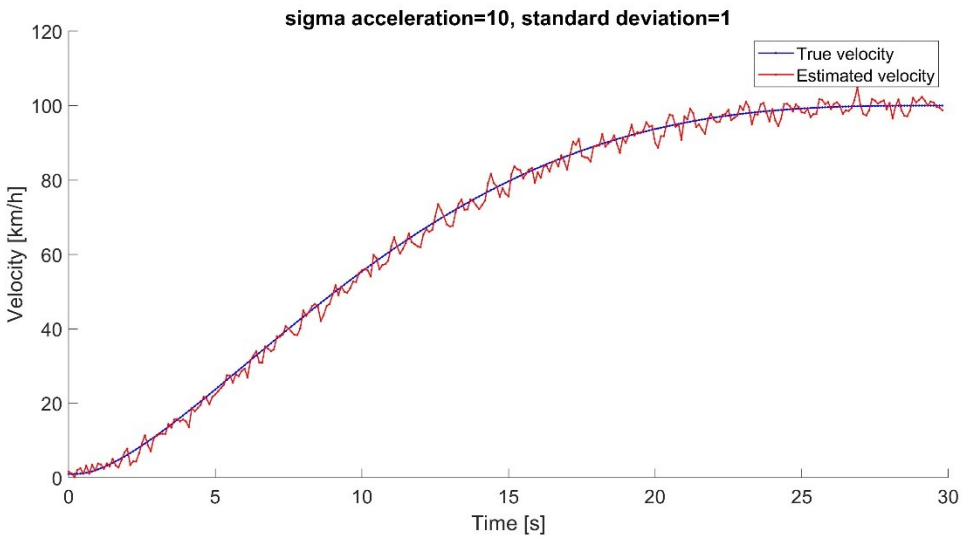

Figure 24. *Velocity estimation for increased σ_{acc}, σ_{pos}=1, σ_{acc}=10*

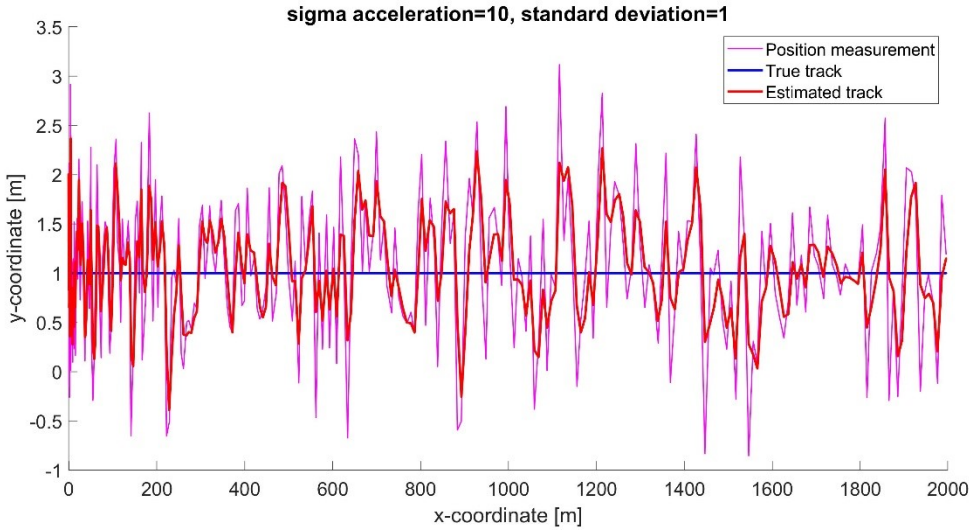

Figure 25. *Degradation in position estimate for increased σ_{acc}, σ_{pos}=1, σ_{acc}=10*

Noticeably, with increased σ_{acc} velocity, estimation curve follows the true velocity in more strict manner as seen in Figure 20.

Finally, a trade-off is adopted for car mobility model scenario where more reasonable value of σ_{acc} is considered as well as standard deviation of position measurement error, σ_{pos} is considered as constant valued one. The phenomenon is illustrated in Figure 26 and 27.

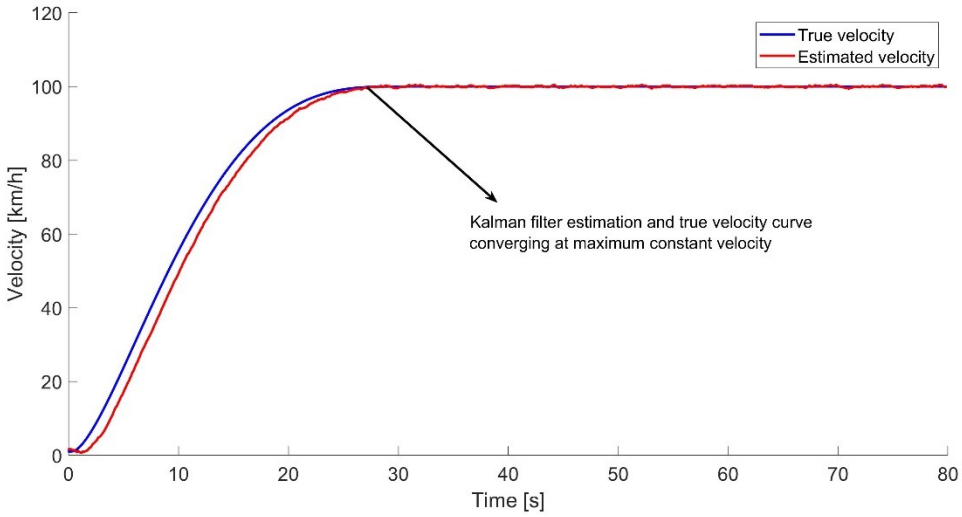

Figure 26. *Trade off scenario for velocity estimation, σ_{pos}=1, σ_{acc}=0.5*

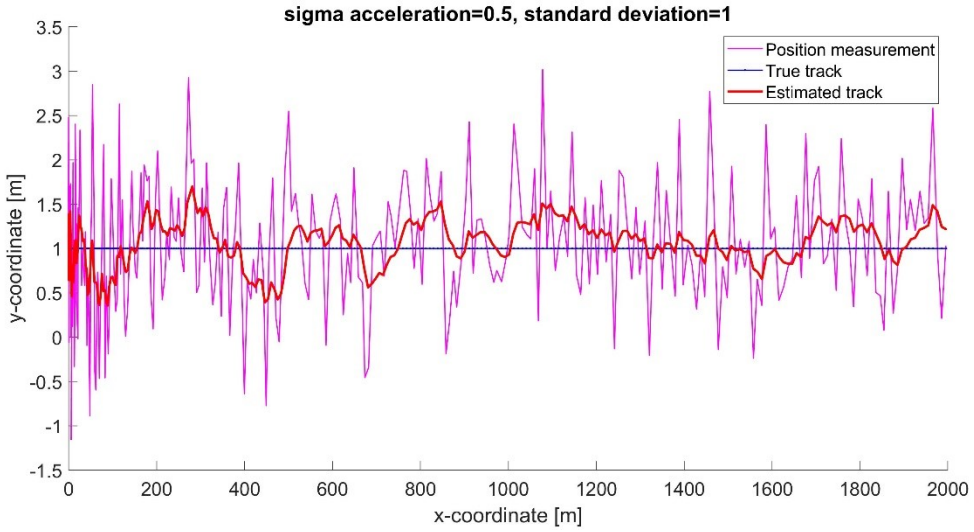

Figure 27. *Increased Position estimation accuracy for reasonable σ_{acc}, σ_{pos}=1, σ_{acc}=0.5*

As seen from Figure 26, estimation for velocity converges with the true velocity once the velocity becomes constant. However, during accelerating period of a vehicle estimation follows the true velocity curve without complete convergence. Moreover, position estimation accuracy increases as lower σ_{pos} as well as reasonable σ_{acc} value comes together in Figure 27. Noticeably, in all Kalman filter output figures for both velocity and position estimates there is an initial delay to merge with the true velocity and position data as a resultant of not providing the filter with true initial estimates.

4.2.2 Train mobility model analysis through Kalman filter

A train mobility model is developed through the element increment method developed by Xu et al, (2016). For analysing the estimation effect of Kalman filter on the train mobility model the initial speed is assumed zero where the final maximum speed is 200 km/h. The model estimates the train taking approximately 2000 m or 2 km to reach the final speed of 200 km/h. From the train mobility model algorithm, the mass of the train is significant for calculating net pulling force of a train. For the simulation scenario Talgo 350 train weighing 322 Tons [29] is considered. Similar simulation approach as mentioned for car mobility model simulation is considered for train simulation scenario as well. Noticeably, Kalman filter velocity estimation curve takes longer to follow the true velocity curve as a result of train taking larger time duration to reach constant maximum velocity. Besides, the pulling force is larger before the train reaches maximum constant velocity resulting in acceleration. However, train acceleration is different from car acceleration as acceleration for train is more uniform in nature. This phenomenon results in a gradual raising curve before achieving maximum velocity. In Figure 28, Kalman filter velocity estimation and true velocity curve is shown.

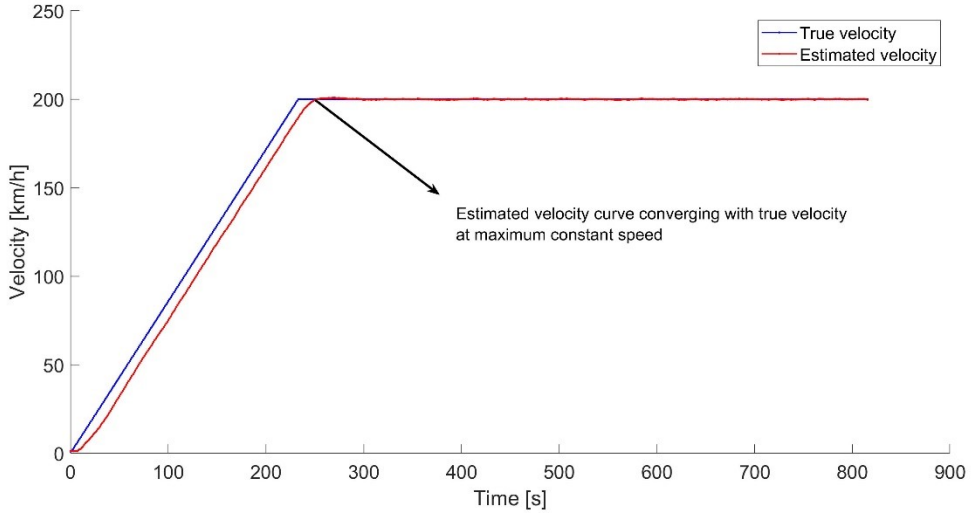

Figure 28. *Estimated velocity curve following true velocity curve, σ_{pos}=1, σ_{acc}=0.5*

Moreover, with increased sigma acceleration value estimated velocity curve follows the true velocity curve more restrictedly as shown in Figure 28. Although, increasing the parameter effecting the estimation oscillation, σ_{acc}, results in better velocity estimation, higher oscillation makes position estimation more difficult as shown in Figure 29 and Figure 30.

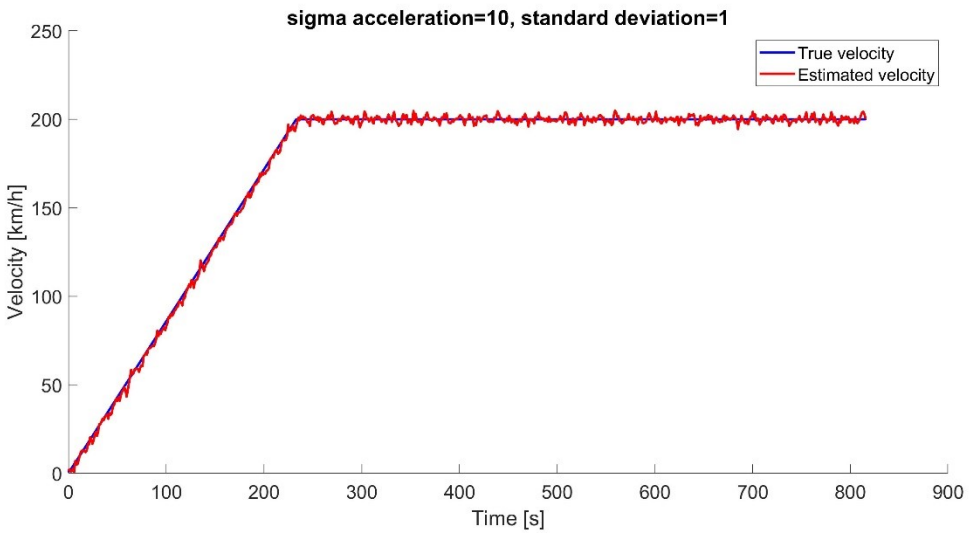

Figure 29. *Estimated velocity following true velocity with increased σ_{acc} , σ_{pos}=1, σ_{acc}=10*

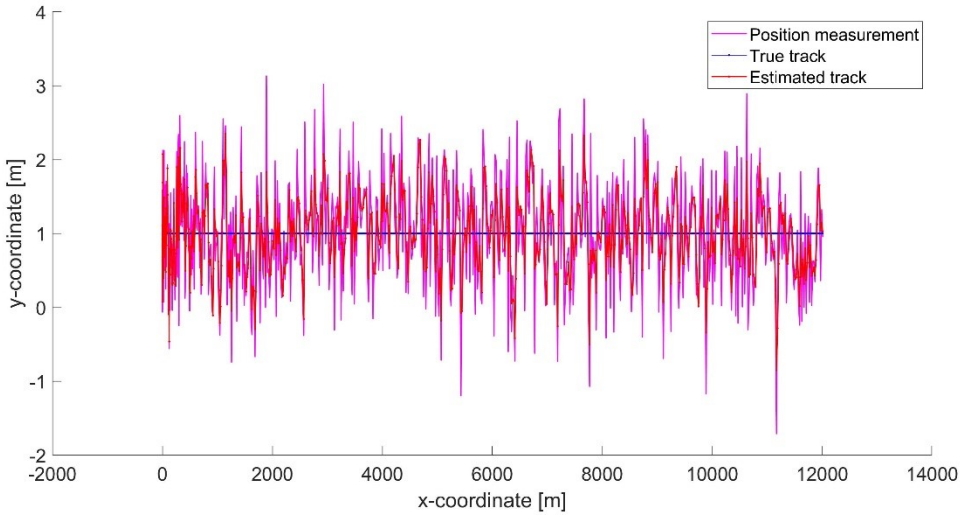

Figure 30. *Degraded position measurement due to oscillation with increased σ_{acc}, σ_{pos}=1, σ_{acc}=10*

5. CHANNEL SIMULATION IN HIGH-SPEED VEHICLE SCENARIO

5.1 Velocity Effect on Doppler shift

In the context of mobility, velocity and carrier frequency are two prime parameters in calculating maximum Doppler shift. However, from equation (1.11), there is another parameter, angle between the receiver and incident wave defining whether the Doppler shift is positive or negative. For the simulation scenario, a vehicle is considered to be moving along x-axis and crossing a base station along the path. The simulation scenario is graphically illustrated in Figure 31.

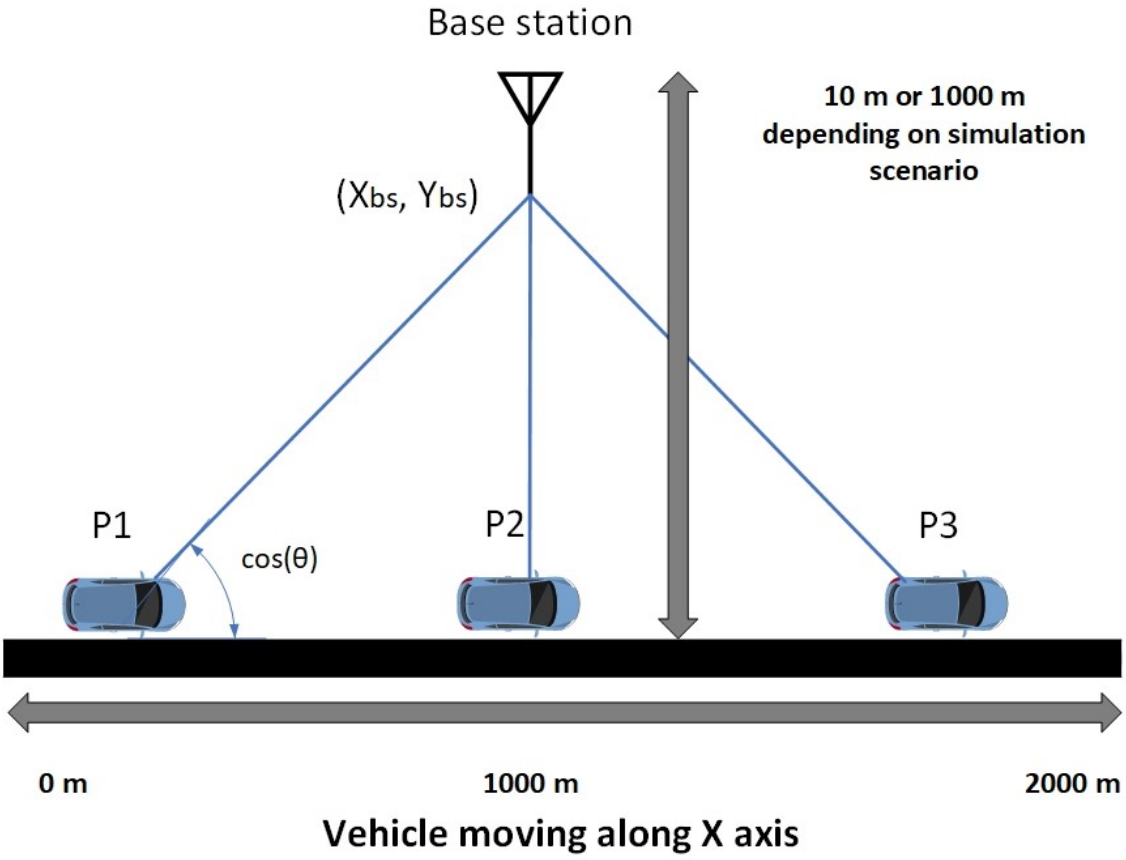

Figure 31. *Simulation scenario in the context of angle between vehicle and base station*

In Figure 31, three vehicle position is noted, namely **P1, P2** and **P3**, to show three phases of Doppler shift, namely, positive, zero crossing and negative. Noticeably, the mentioned scenario depends on the angle θ.

In the simulation, regarding velocity both accelerating and constant velocity is considered for the vehicle. For accelerating vehicle scenario, a vehicle is considered to move from zero initial velocity to final velocity of 100 km/h while covering a distance of 2000m. Again, for a vehicle moving with constant velocity, the vehicle moves along the same path with a constant velocity of 100 km/h. Besides, the approach is simulated on two different carrier frequencies, 3.5 GHz and 30 GHz. The simulation outcome is shown in Figure 32.

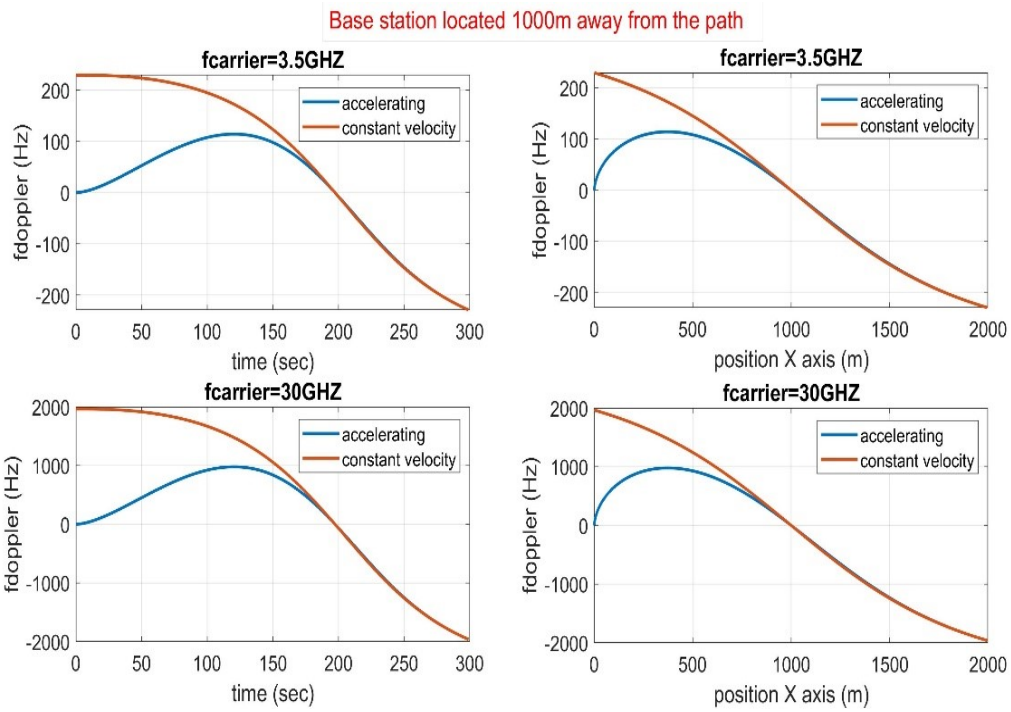

Figure 32. *Doppler shift scenario for X_{bs} = 1000 m, Y_{bs} =1000m*

From Figure 29, the difference between an accelerating vehicle and a vehicle moving with constant velocity being the initial velocity effects the Doppler shift curve similarly. In the simulation scenario the base station is located 1000 m away from the path while the vehicle crosses it. The positive Doppler shift values before crossing the base station depict that the vehicle is moving towards the base station. Again, at the instance of vehicle crossing the base station the Doppler shift value becomes zero. Finally, the Doppler shift values becomes negative after the vehicle crosses past the base station depicting that the vehicle is moving away from the base station.

The same scenario mentioned before is again simulated with a base station located only 10 m away from the vehicle path. The simulation outcome is illustrated in Figure 33.

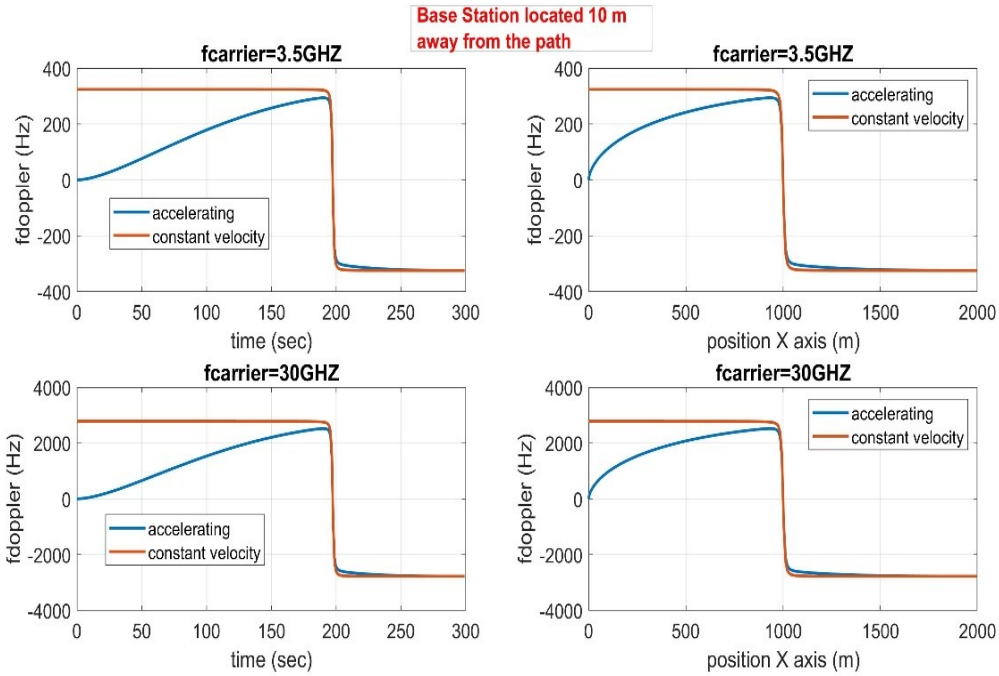

Figure 33. *Doppler shift scenario for X_{bs} = 1000 m, Y_{bs} = 10m*

From Figure 32 and Figure 33, difference in Doppler shift curve lies at the zero crossing point. Doppler shift curve smoothly crosses the zero point for a distant base station from the vehicle path whereas, for a base station located near, the Doppler shift curve crosses the zero point in abrupt manner. The phenomenon is furthermore explained by the angle between the receiver reference plane and incident wave. Noticeably, the angle is dependent on the distance between the transmitter and receiver reference plane. For a distant base station, the angle changes in smooth manner resulting in a smooth Doppler shift curve. However, for a base station located near the receiver reference plane or vehicle path in the context of simulation, the angle change is more abrupt in nature resulting in an abrupt change in Doppler shift curve. Finally, apart from the velocity of the vehicle, system geometry of transmitter and receiver i.e. the distance and angle between them affects the Doppler shift.

5.2 Velocity Effect on Channel Fading

Channel fading being the resultant of multipath phenomenon, velocity affects the channel fading through maximum Doppler shift. Besides, maximum Doppler shift depends on velocity of user equipment as well as carrier frequency of the channel. The simulation scenario is designed for two different carrier frequencies, 3.5 GHz and 30 GHz both suitable for 5G New Radio [47]. Constant velocity for three different scenarios, pedestrian, car

and train is considered to be 5 km/h, 100 km/h and 200 km/h accordingly. The simulation output is illustrated in Figure 34,

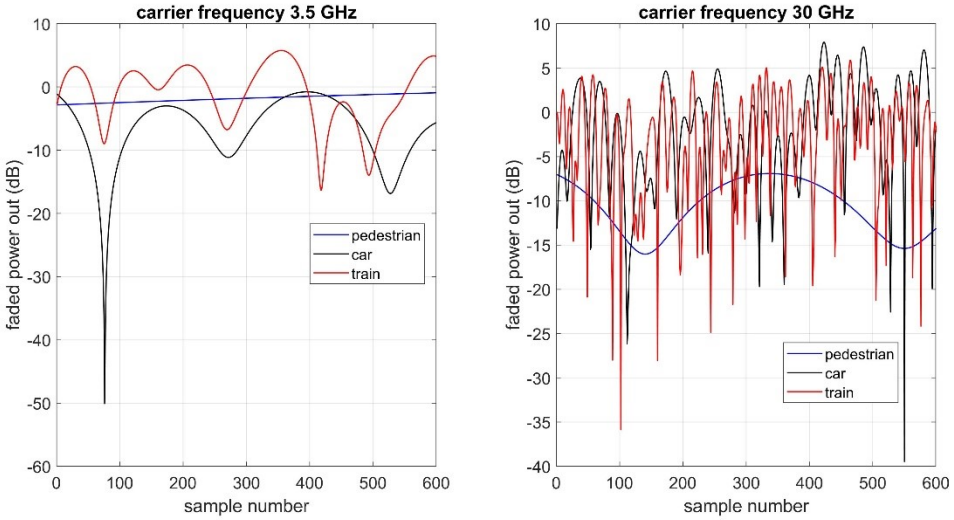

Figure 34. *Fading as a function of velocity and carrier frequency*

As seen in Figure 34, while using 3.5 GHz carrier frequency, fading rate for pedestrian is relatively low compared to car and train fading profiles. Moreover, car fading profile is varying in higher rate than the train fading profile. However, with 30 GHz carrier frequency the fading profiles are intensified with higher fading rate. Moreover, the effect of fading is dominant for even lower velocity while higher carrier frequency is in use.

6. CONCLUSION

The aim of this thesis is to study the mobility models regarding different vehicle types as well as select suitable mobility models from a realistic and analytical point of view. Mobility models are required to define the behaviour of different types of vehicles during acceleration, deceleration as well as turning and following other vehicles. In addition, the selected mobility models are analyzed and simulated to illustrate the effect of mobility on wireless channel modelling parameters. Moreover, evaluation of channel performance is performed through channel modelling parameter analysis in the context of user equipment mobility. Additionally, for tracking user position with velocity estimates, data is collected from the simulation scenario of different mobility models and is used as input to the Kalman filter to illustrate effect of mobility on the tracking performance. Finally, Different simulation scenarios are repeated with different carrier frequencies to demonstrate the effect of different carrier frequency usage on channel parameters regarding mobility of the user.

Communication channel model and considered parameters are described and analysed through simulation in the context of user's mobility. Regarding channel modelling principles, path loss models are described based on the Okumura-Hata model and the 3GPP-specified urban macro scenario to illustrate both line of sight and non-line of sight path loss models. Moreover, urban macro scenario is considered, as the simulation environment converges well with the mobility model representation. Besides, channel parameters in close convergence with user mobility, like Doppler effect, delay spread, coherence time and coherence bandwidth, are described and analysed through simulation on different velocities as well as different carrier frequencies. Firstly, Doppler effect is described through maximum Doppler frequency shift as well as Doppler spectrum where the simulation outputs illustrate that both higher carrier frequency and higher velocity result in greater maximum Doppler frequency shift. Besides, spreading of Doppler spectrum increases as a resultant of previous mentioned phenomenon. Secondly, delay spread in communication channel is observed as a resultant of multipath phenomenon, where the amount of delay spread is dependent on the area of propagation. However, delay spread is observed to be different in indoor and outdoor environments as a result of difference in reflector characteristics as well as difference in receiver location. Thirdly, regarding coherence time, with larger carrier frequency and greater velocity of user, channel coherence time becomes smaller resulting in more frequent time update for the

communication channel. Finally, with higher mobility of transceivers defining transmission matrix for MIMO systems becomes complicated as a resultant of increase in transmission paths between transmitter and receivers.

Mobility models designed for different vehicle types as well as for pedestrian mobility is studied and analysed through simulation in a comparative nature, where the first noticeable parameter is the degree of freedom of mobility. However, increase in degree of freedom introduces increased randomness to the mobility model designing. As a result, mobility models for airborne networks as well as for pedestrians are designed by taking measures for reducing randomness in the modelling algorithm. Conversely, mobility for cars and high speed trains is more restricted because of the traffic regulations, following of predetermined roads or tracks as well as comparatively larger mass of the vehicle. During the study and simulation of different mobility models, single vehicle mobility is considered for simplicity as well as mobility model algorithm restriction. The velocity and position data are achieved from the mobility models and provided as input to the Kalman filter to analyse the effect of mobility on user position tracking as well as achieving velocity estimates. As seen from observing simulation output, Kalman filter estimation works better when the vehicle is moving with a constant speed rather than accelerating or decelerating.

In the context of ground based vehicular mobility, like cars, simple acceleration and deceleration model is considered. For simplicity of mobility model representation, specific traffic scenarios like roundabouts, traffic intersections, traffic demand level as well as road types are not considered in this thesis scope. However, concerning future research aspects, various scenarios as mentioned can be considered to design mobility models in a more efficient and realistic way. Moreover, realistic model for simulating multiple different vehicles in various traffic scenarios should be designed based on vehicle following behaviour, safety measures during lane changing as well as bending of tracks or roads. Additionally, for high speed trains, a simple simulation scenario is considered where the high speed train accelerates to a maximum constant speed and continues coasting at the constant speed. Concerning airborne vehicular mobility models, critical research is needed for model validation, identification of better model granularity as well as evaluation of airborne network performance aspects and efficient network designing. Therefore, large airborne field data is required to validate and parameterize mobility models to decide optimal model granularity. Moreover, for designing mobility models for multiple unmanned aerial vehicles in close vicinity, collision avoidance between UAVs should be considered by making particular UAV aware of other airborne paths. Finally, detailed study of the mobility models along with analysing the simulation results through

real time traffic data will provide a solid ground for future positioning and communications studies.

REFERENCES

[1] M. L. Sichitiu, "Mobility models for ad hoc networks," in *Guide to Wireless Ad Hoc Networks*Anonymous 2009, .

[2] H. Liu and B. Zhu, *Formation Control of Multiple Autonomous Vehicle Systems.* (1st edition ed.) 2018Available: https://tuni.finna.fi/Record/oma.823494.

[3] C. Wang *et al*, "Channel measurements and models for high-speed train communication systems: A survey," *IEEE Communications Surveys & Tutorials,* vol. 18, *(2),* pp. 974-987, 2015.

[4] *Simulate channel models for wireless communication*. Available: https://se.mathworks.com/discovery/channel-model.html.

[5] A. F. Molisch, *Wireless Communications.* (2. ed., reprinted ed.) 2011.

[6] F. Belloni, "Physical Layer Methods in Wireless Communication Systems," *Fading Models Course, Helsinki University of Technology, November,* 2004. Available: http://www.comlab.hut.fi/opetus/333/2004_2005_slides/Path_loss_models.

[7] 3GPP TR 38.901, "3rd Generation Partnership Project;
Technical Specification Group Radio Access Network;
Study on channel model for frequencies from 0.5 to 100 GHz (Release 16) " 10.10., 2019.

[8] S. Anandamurugan and P. S. Nandhini, *Wireless Networks.* 2016Available: http://search.ebscohost.com/login.aspx?direct=true&AuthType=cookie,ip,uid&db=nlebk&AN=1385389&site=ehost-live&scope=site&authtype=sso&custid=s4778523.

[9] (). *Fast fading vs slow fading-difference between fast,slow fading*. Available: https://www.rfwireless-world.com/Terminology/fast-fading-vs-slow-fading.html.

[10] Theodore S. Rappaport, *Wireless Communications Principles and Practice, Second Edition.* (Second ed.) 2001.

[11] W. C. Jakes, *Microwave Mobile Communications.* New York u.a: Wiley, 1974.

[12] T. S. Rappaport, K. Blankenship and H. Xu, "Propagation and radio system design issues in mobile radio systems for the glomo project," Available: https://www.researchgate.net/publication/247282643_Propagation_and_radio_system_design_issues_in_mobile_radio_systems_for_the_glomo_project.

[13] A. A. Saleh and R. Valenzuela, "A statistical model for indoor multipath propagation," *IEEE J. Select. Areas Commun.,* vol. 5, *(2),* pp. 128-137, 1987.

[14] D. Devasirvatham *et al*, "Radio propagation measurements at 850 MHz, 1.7 GHz and 4 GHz inside two dissimilar office buildings," *Electron. Lett.,* vol. 26, *(7),* pp. 445-447, 1990.

[15] S. Y. Seidel *et al*, "The impact of surrounding buildings on propagation for wireless in-building personal communications system design," in *[1992 Proceedings] Vehicular Technology Society 42nd VTS Conference-Frontiers of Technology,* 1992, .

[16] D. Cox and R. Leck, "Distributions of multipath delay spread and average excess delay for 910-MHz urban mobile radio paths," *IEEE Transactions on Antennas and Propagation,* vol. 23, *(2),* pp. 206-213, 1975.

[17] T. S. Rappaport, S. Y. Seidel and R. Singh, "900-MHz multipath propagation measurements for US digital cellular radiotelephone," *IEEE Transactions on Vehicular Technology,* vol. 39, *(2),* pp. 132-139, 1990.

[18] (). *Coherence Bandwidth and Coherence Time*. Available: https://www.rfwireless-world.com/Terminology/Coherence-Bandwidth-Coherence-Time.html.

[19] J. Sharony, "Introduction to wireless MIMO–theory and applications," *CEWIT—Center of Excellence in Wireless and Informational Technology, Stony Brook University, IEEE LI,* 2006.

[20] A. N. Barreto *et al*, "5G–wireless communications for 2020," *Journal of Communication and Information Systems,* vol. 31, *(1),* 2016.

[21] Cheolhee Park and T. S. Rappaport, "Short-Range Wireless Communications for Next-Generation Networks: UWB, 60 GHz Millimeter-Wave WPAN, And ZigBee," *Wc-M,* vol. 14, *(4),* pp. 70-78, 2007. Available: https://ieeexplore.ieee.org/document/4300986. DOI: 10.1109/MWC.2007.4300986.

[22] M. Martinez-Ingles *et al*, "Experimental comparison between centimeter- and millimeter-wave ultrawideband radio channels," *Radio Science,* vol. 49, *(6),* pp. 450-458, 2014. . DOI: 10.1002/2014RS005439.

[23] R. Akçelik and M. Besley, "Acceleration and deceleration models," in *23rd Conference of Australian Institutes of Transport Research (CAITR 2001), Monash University, Melbourne, Australia,* 2001, .

[24] G. Xu *et al*, "Train movement simulation by element increment method," *Journal of Advanced Transportation,* vol. 50, *(8),* pp. 2060-2076, 2016. . DOI: 10.1002/atr.1445.

[25] Junfei Xie *et al*, "A Survey and Analysis of Mobility Models for Airborne Networks," *Comst,* vol. 16, *(3),* pp. 1221-1238, 2014. Available: https://ieeexplore.ieee.org/document/6689509. DOI: 10.1109/SURV.2013.111313.00138.

[26] J. G. Carrillo-González, J. Arámburo-Lizárraga and R. Ortega-Magaña, "Modeling the Turning Speed and Car Following Behaviors of Autonomous Vehicles in a Virtual World," *Ingeniería, Investigación Y Tecnología,* vol. 16, *(3),* pp. 391-405, 2015. Available: http://www.scielo.org.mx/scielo.php?script=sci_arttext&pid=S1405-77432015000300007&lng=en&tlng=en.

[27] K. Li, Z. Gao and B. Ning, "Cellular automaton model for railway traffic," *Journal of Computational Physics,* vol. 209, *(1),* pp. 179-192, 2005.

[28] Z. Rao, "Train traction calculation," *China Railway, Beijing, China,* 2005.

[29] C. CERECEDA GARCIA, "Talgo evolves its unique design for ultra high speed," *Int. Railway J.,* vol. 42, *(10),* 2002.

[30] J. Xie *et al*, "A survey and analysis of mobility models for airborne networks," *IEEE Communications Surveys & Tutorials,* vol. 16, *(3),* pp. 1221-1238, 2013.

[31] Y. Wang and Y. J. Zhao, "Fundamental issues in systematic design of airborne networks for aviation," in *2006 IEEE Aerospace Conference,* 2006, .

[32] N. Aschenbruck, E. Gerhards-Padilla and P. Martini, "A survey on mobility models for performance analysis in tactical mobile networks," *Journal of Telecommunications and Information Technology,* pp. 54-61, 2008.

[33] F. Bai and A. Helmy, "A survey of mobility modeling and analysis in wireless," *Wireless Ad Hoc and Sensor Networks,* 2006.

[34] K. Namuduri *et al*, "Airborne network: A cyber-physical system perspective," in *Proceedings of the First ACM MobiHoc Workshop on Airborne Networks and Communications,* 2012, .

[35] T. Saadawi, "No title," *Optimizing Airborne Networking Performance with Cross-Layer Design Approach,* 2009.

[36] T. Saadawi, "No title," *A Delay Tolerant Networking Architecture for Airborne Networking,* 2010.

[37] T. Camp, J. Boleng and V. Davies, "A survey of mobility models for ad hoc network research," *Wireless Communications and Mobile Computing,* vol. 2, *(5),* pp. 483-502, 2002.

[38] D. B. Johnson and D. A. Maltz, "Dynamic source routing in ad hoc wireless networks," in *Mobile Computing*Anonymous 1996, .

[39] E. M. Royer, P. M. Melliar-Smith and L. E. Moser, "An analysis of the optimum node density for ad hoc mobile networks," in *ICC 2001. IEEE International Conference on Communications. Conference Record (Cat. no. 01CH37240),* 2001, .

[40] Y. Hu and D. B. Johnson, "Caching strategies in on-demand routing protocols for wireless ad hoc networks," in *Proceedings of the 6th Annual International Conference on Mobile Computing and Networking,* 2000, .

[41] V. Tolety, "Load reduction in ad hoc networks using mobile servers," 1999.

[42] R. A. Singer, "Estimating optimal tracking filter performance for manned maneuvering targets," *IEEE Trans. Aerospace Electron. Syst., (4),* pp. 473-483, 1970.

[43] A. Papoulis and S. U. Pillai, *Probability, Random Variables, and Stochastic Processes.* 2002.

[44] D. Broyles, A. Jabbar and J. P. Sterbenz, "Design and analysis of a 3–D gauss-markov mobility model for highly-dynamic airborne networks," in *Proceedings of the International Telemetering Conference (ITC), San Diego, CA,* 2010, .

[45] D. K. Patil and B. V. Khode, "Effect of Pedestrian Movement on Traffic Los," *IJSTE - International Journal of Science Technology & Engineering,* vol. 3, *(9),* 2017. Available: https://pdfs.semanticscholar.org/909f/b27b91f5771c48dd4ffc872ac6760246d84f.pdf.

[46] B. Ristic, S. Arulampalam and N. Gordon, *Beyond the Kalman Filter.* 2004.

[47] E. Dahlman, S. Parkvall and J. Skold, *5G NR: The Next Generation Wireless Access Technology.* 2018.